Intrazeolite Organometallics and Coordination Complexes: Internal versus External Confinement of Metal Guests

GEOFFREY A. OZIN* and CAROLINE GIL†

Lash Miller Chemical Laboratories, University of Toronto, 80 St. George Street, Toronto, Ontario, Canada, M5S 1A1

Received September 23, 1988 (Revised Manuscript Received July 24, 1989)

Contents

A. Introduction

A wide variety of metal clusters, organometallic compounds, and coordination compounds have been encapsulated in a range of different zeolite hosts. These composite materials have found numerous applications, including size/shape-selective catalysis, gas separation/purification, artificial photosynthesis, and electro- and photocatalysis.

In the context of catalysis, increased efforts have been set forth in the immobilization of known homogeneous catalysts on solid supports such as silica, alumina, and polymers.[1] Under ideal circumstances, such a hybrid catalyst would combine the advantages of homogeneous and heterogeneous catalysts while minimizing the disadvantages of both. It is hoped that comparable activity to solution phase would be accompanied by equivalent or enhanced selectivity. Also, the ease of separation and purification of reactants, products, and catalysts on the heterogeneous systems, in principle, provides an attractive advantage over homogeneous systems. Finally, the ability to work at elevated temperatures would tend to overcome any diffusional impediments of the incorporated species as well as promote reactions with high activation barriers.

In this regard the intracrystalline cage and channel structure of zeolites has long attracted researchers interested in developing well-characterized heterogeneous catalyst systems. The framework structures of some commonly studied zeolites are represented in Figure 1. These microporous aluminosilicates are composed of SiO_4 and AlO_4^- tetrahedra joined through shared oxygen bridges. The large cavity in these zeolites is typically referred to as the α-cage while the smaller cavities are known as β-cages. The net negative charge on the lattice is counterbalanced by exchangeable cations located at well-defined sites which are labeled in Figure 1 according to convention. Protons may also act as the charge-balancing cation. These acid zeolites may be

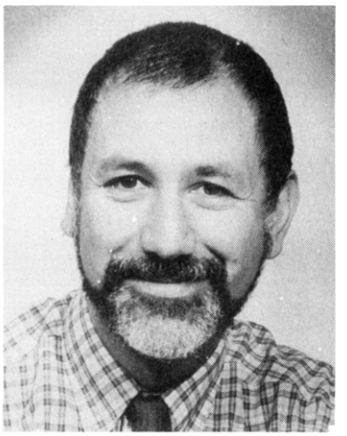

Geoffrey A. Ozin was born in London, England, in 1943; he completed his undergraduate work in chemistry at King's College, London University, obtained his D.Phil. degree in inorganic chemistry at Oriel College, Oxford University, in 1967, and was an ICI Postdoctoral Fellow at Southampton University from 1967 to 1969. He joined the chemistry faculty of the University of Toronto as an Assistant Professor in 1969, where he is now a Full Professor. His current research is exclusively in the area of solid-state chemistry with a thrust toward advanced zeolite materials science. The emphasis of his work is on the synthesis and characterization of novel microporous materials with structure–property–function organized for the development of systems with value in data storage, size/shape-discriminating chemical sensing, and artificial structures.

Caroline Gil received her B.Sc. degree (1985) and M.Sc. degree (1988, with Dr. G. A. Ozin) from the University of Toronto. After working for a year as a chemist for Colgate-Palmolive Canada, she is now pursuing a Ph.D. at MIT, Boston.

* Author to whom correspondence should be addressed.
† Present address: Chemistry Department, MIT, Boston, MA 02139.

0009-2665/89/0789-1749$06.50/0

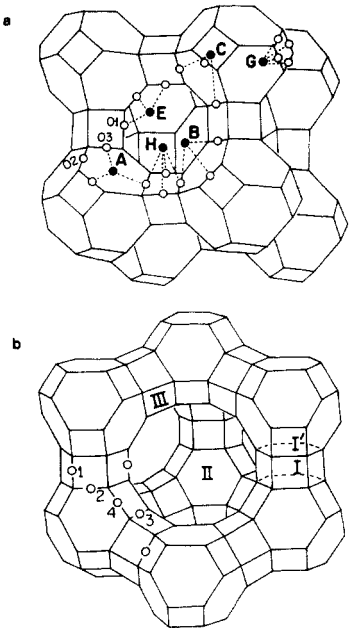

Figure 1. Framework structure of (a) zeolite A and (b) faujasite zeolites X and Y. Every vertex represents an aluminum or silicon atom; oxygen bridges are not shown. Extraframework cation locations are shown and labeled according to convention. Reprinted from ref 2; copyright 1974 John Wiley & Sons, Inc.

formed by the gradual dehydration/deammination of ammonium cation exchanged zeolites. Materials of this type are attractive hosts for catalytic species due to their high thermal stability, well-defined structure, large internal surface area, and potential to impose size and shape selectivity on the product distribution due to the molecular sieving effect of zeolites.[2]

The unique advantages of zeolites are obvious. Rapid and significant developments involving the synthesis, characterization, and structure–property relationships of intrazeolite organometallics and coordination compounds have been realized in recent years. Zeolites, like any other solid-state material, have their limitations. Those specific to zeolites include pore plugging, poisoning, migration, leaching, and structural defects involving reactants, products, catalytic guest, and zeolite host.

Thus the ideal state of affairs alluded to above is not usually experienced in practice as real working systems have demonstrated. For example, metal guests can migrate to the external surface of the host to produce deleterious aggregation or leaching effects. The separation/purification of reactants, products, and catalysts can sometimes prove to be problematical. Catalytic turnovers may be severely limited by clogging of pores by products, therefore necessitating frequent catalyst regeneration operations. The latter may require high-temperature methods which may create difficulties when the immobilized metal guest is intrinsically unstable. Although diffusional problems involving reactants and products may be overcome by working at elevated temperatures, one can introduce diffusional difficulties associated with the so-called immobilized metal guest. Although many of these problems can be solved, one needs to recognize the strengths and weaknesses when comtemplating potential technological applications of this class of materials.

A central issue pervading studies of the aforementioned systems is the ability to conduct experiments

TABLE 1. Summary of Synthetic Methods for Preparing Intrazeolite Metal Clusters ($M_n^{q+}Z$)[a]

precursor	method	ref
$M^{p+}Z$	thermal reduction with H_2, CO	73
	photochemical reduction, H_2	8
	H atom reduction (microwave)	8
	MVS solution phase	6
	reduction with Na, Cd vapor	73
	autoreduction, H_2O	73
$MX_n^{r+}Z$	autoreduction, X = H_2O, NH_3	73
	thermal reduction, H_2	13
	electrochemical reduction	72
ML_nZ	thermal ligand loss	5, 11
	photochemical ligand loss	73
	microwave discharge	7
	$NaBH_4$ reduction, $Pt(acac)_2$	13

[a] M^{p+} = extraframework reducible cation; MX_n^{r+} = extraframework reducible complex; ML_n = encapsulated organometallic molecule or fragment; M_n^{q+} = encapsulated metal cluster.

TABLE 2. Summary of Synthetic Methods for Preparing Intrazeolite Metal Complexes ($MX_n^{r+}Z$)

precursor	method	ref
M^{p+}	intrazeolite ligation	42–46
	intrazeolite ligand assembly	59, 60
	ligand exchange followed by ion exchange	52
Na^+Z	ion exchange of MX_n^{r+}	70, 73

TABLE 3. Summary of Synthetic Methods for Preparing Intrazeolite Organometallics (ML_nZ)

precursor	method	ref
$M^{p+}Z$	vapor-phase sublimation, ML_n	36
	solution-phase impregnation, ML_n	27
	intrazeolite ligation	15
	MVS solution phase	6
$MX_n^{r+}Z$	intrazeolite ligand exchange, reductive ligation	15
ML_nZ	intrazeolite organometallic transformations	62
$M_n^{q+}Z$	intrazeolite cluster/ligand reactions	73

that intentionally target the metal guest in the internal channels and/or cavities of the zeolite host rather than on the external surface of the zeolite crystals. Also, the attainment of a homogeneous distribution of the metal guest throughout the bulk of the zeolite host crystal, instead of being concentrated in the external surface regions or inhomogeneously arranged in the zeolite, is a desirable goal in the preparation of well-defined materials.

In many of the metal/zeolite systems recently examined a central issue is the internal versus external confinement and the distribution of the metal guest in the zeolite host. Under appropriate conditions the internal entrapment of the guest can be achieved and ascertained by several physical and chemical methods, some of which are listed below and summarized in Scheme 1: (i) size exclusion involving both guest and host variations; (ii) size/shape-discerning chemical/catalytic reactions; (iii) size-dependent poisoning reactions; (iv) mid-IR vibrational symmetry/frequency perturbations of the guest molecule; (v) perturbations of the far-IR cation translatory modes by the guest; (vi) EPR and NMR relaxation effects; (vii) surface- and bulk-sensitive spectroscopy, microscopy, and diffraction probes (e.g., XPS, TEM, and XRD); (viii) spatially resolved intrazeolite redox titrations involving Brønsted acid sites.

Examples of these methods in use will be given throughout the text. For convenience divisions have been made based on the type of intrazeolite guest,

SCHEME 1. Internal versus External Probes of Metal Guests in Zeolites

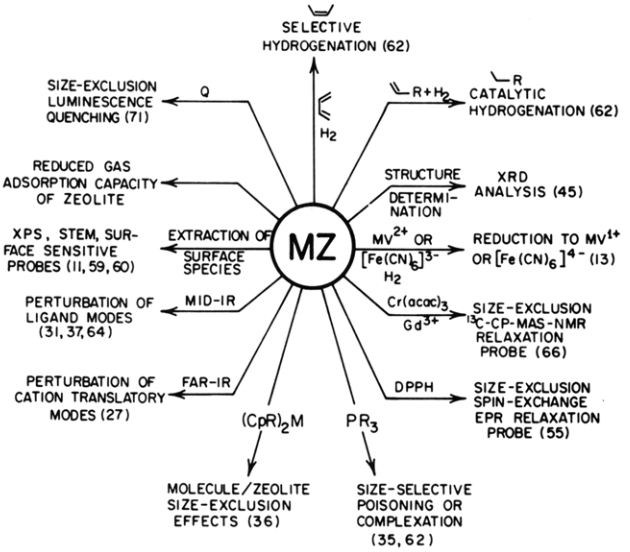

namely, metal clusters, carbonyl compounds, coordination compounds, and organometallics. A brief summary of the synthetic methods used to encapsulate these compounds is given in Tables 1–3.

B. Metal Clusters

Much of the initial work with zeolite catalysts focused on the properties of the zeolite itself. In particular, the acid-exchanged forms are widely used as cracking catalysts.[3] A major goal has also been to produce metal clusters within the large spatially accessible pores of primarily zeolites X and Y.[4] Various methods have been used in this field, including the decomposition of small carbonyl clusters incorporated into the supercage,[5] solution-phase metal atom impregnation,[6] in situ microwave decomposition of encapsulated organometallics,[7] and reduction of extraframework transition-metal cations such as the reduction of Ni^{2+} in NaX by molecular hydrogen or hydrogen atom beams.[8] A summary of these methods is given in Table 1.

Small metal particles can be formed within the α-cages of faujasites by the decomposition/reduction of encaged carbonyl clusters. Although major difficulties exist with this approach, such as metal cluster formation, migration to the external surface, and subsequent agglomeration and accompanying redox processes, considerable success has been achieved in this area. For example, adsorption of $Re_2(CO)_{10}$ and $Ru_3(CO)_{12}$ into HY[9] followed by decarbonylation leads to the formation of highly dispersed metal particles inside the zeolite host.

More recently, the progressive decomposition of $Mo(CO)_6$ in HY and NaY has been followed by EPR and IR measurements.[10] In the acid zeolite various subcarbonyl species form at low temperatures. At higher activation temperatures Mo^+ forms and subsequently three distinct Mo^{5+} moieties are observed by their diagnostic EPR signals. In NaY only one subcarbonyl species is observed during decomposition while higher tempeatures lead to metallic molybdenum. X-ray diffraction and electron microscopy clearly indicate that the molybdenum clusters are not on the outer surface of the zeolite.[11] In addition, XPS and

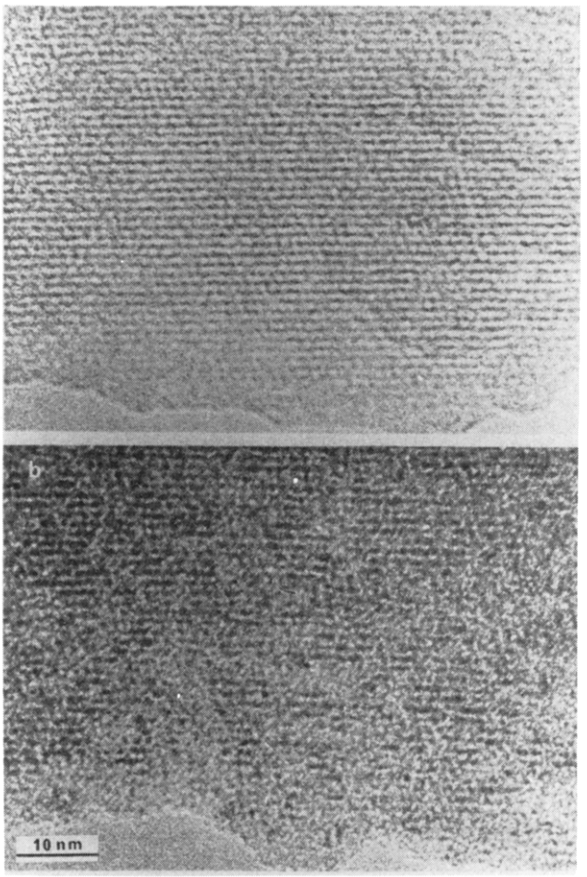

Figure 2. Transmission electron micrographs of (a) unloaded NaY zeolite and (b) MoNaY zeolite with 95 Mo per unit cell. Mo particles are identified by high-contrast spots along what appear to be the remnants of the lattice images. Reprinted from ref 12a; copyright 1987 American Chemical Society.

TEM data show that the zerovalent molybdenum clusters formed are uniformly dispersed throughout the zeolite crystal (Figure 2).[12] The 1–1.2-eV high-energy shift of the molybdenum 3d core level binding energies, relative to bulk metal, in the absence of oxidation is attributed to quantum size effects of sub-12-Å molybdenum clusters (Figure 3).

A chemical means of identifying the location of metal clusters has recently been demonstrated for platinum particles in Y and L zeolites.[13] The particles were formed in three different ways: (i) exchange with $[Pt(NH_3)_4]^{2+}$ followed by reduction with hydrogen, (ii) exchange with $[Pt(NH_3)_4]^{2+}$ followed by reduction with $NaBH_4$, and (iii) exchange with $Pt(acac)_2$ followed by reduction with $NaBH_4$. The last method gives very low loadings of metal, $(1–3) \times 10^{-4}$ mmol/g, while the former methods give variable loadings up to 1×10^{-1}mmol/g. One of the location probe reactions studied was the platinum-catalyzed reduction of methylviologen (MV^{2+}). Reduction of MV^{2+} to the cation radical, $MV^{\bullet+}$, occurs rapidly at pH > 7:

$$MV^{2+} + \tfrac{1}{2}H_2 \rightarrow MV^{\bullet+} + H^+$$

MV^{2+} readily exchanges into Y and L zeolites up to a maximum loading of 1 molecule per large cage while the rest remains in solution. The exchange between zeolite-bound and solution-phase methylviologen is known to be relatively slow. Also, the reduction potential of the $MV^{2+/\bullet+}$ couple is slightly more positive in the zeolite than in solution. Therefore, zeolites that are platinized only internally do not catalyze the reduction

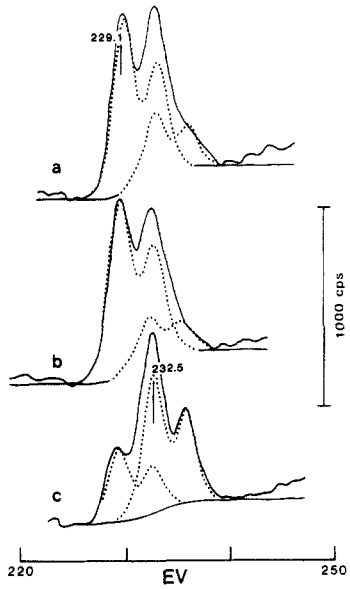

Figure 3. Mo 3d XPS spectra of MoNaY after various treatments, showing the oxidation states identified by curve fitting each spectrum with two doublets: (a) activation in vacuo at 400 °C; (b) reduced in H_2 for 5 min at 400 °C; (c) air-exposed for ~24 h. Reprinted from ref 12b; copyright 1989 American Chemical Society.

of solution-phase MV^{2+}. When the platinum particles generated from $Pt(acac)_2$/L are equilibrated with MV^{2+} followed by the addition of H_2, only the zeolite turned the characteristic blue of the reduced viologen radicals, consistent with only internally localized particles. Conversely, all the other platinized zeolites yielded both blue solutions and blue zeolites when subjected to the same conditions, indicating that platinum particles are located both inside and on the external surface of the zeolite. To further probe this idea the reaction of these systems with $[Fe(CN)_6]^{3-}$ was also investigated. As established by UV–vis spectra, this anionic complex cannot enter the anionic frameworks of either the Y or L zeolites. In the presence of platinum and hydrogen $[Fe(CN)_6]^{3-}$ is reduced to $[Fe(CN)_6]^{4-}$. In a 1×10^{-4} M solution of $[Fe(CN)_6]^{3-}$ the platinum clusters from the $Pt(acac)_2$/)/L system caused no change in the UV–vis spectra of the solution after 6 h of purging with hydrogen. When treated in the same way, the zeolites platinized both inside and outside resulted in a complete disappearance of the characteristic maxima at 302 and 418 nm due to the ferricyanide ion. Clearly, no reduction occurs in the first instance, confirming only internal platinum particles, while in the latter cases externally confined metal particles catalyze the reduction of the ferricyanide ion. Sensitivity test on SiO_2 suggest that in the L zeolite platinized with $Pt(acac)_2$ <0.1% of the platinum is on the external surface. The reduction of $Pt(acac)_2$ by $NaBH_4$ in zeolite L provides a clean and easy way of quantitatively locating small platinum particles only within the zeolite voids. This also demonstrates an easy means of locating metal particles internally or externally provided a fast, easily monitorable chemical reaction exists for the metal under study.

C. Carbonyl Compounds

(i) Homoleptic Carbonyl Compounds

The encapsulation of carbonyl and subcarbonyl

SCHEME 2

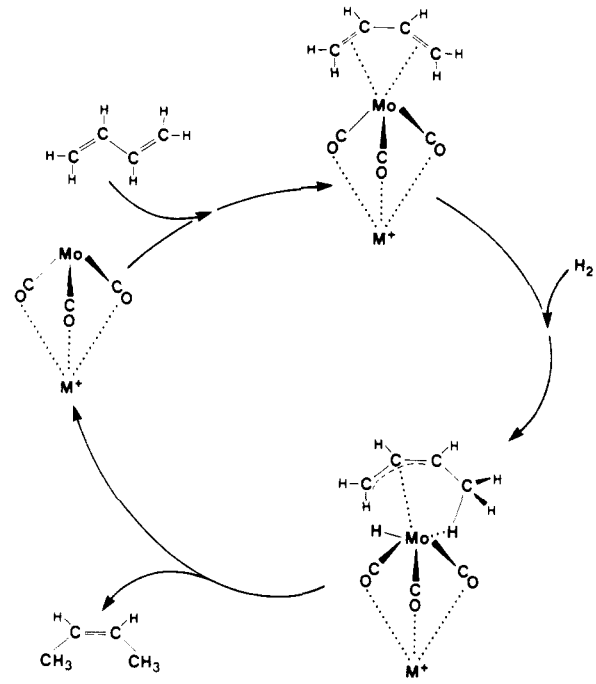

species is of interest because of the catalytic potential of many carbonyl systems. For example, the carbonyl species formed from $Mo(CO)_6$ in M^+Y (M = Li, Na, K, Cs), discussed above, exhibits high activity and selectivity in the hydrogenation of 1,3-butadiene to *cis*-2-butene.[14] Particularly active is a 45% Li^+-exchanged NaY zeolite, Si:Al = 2.78, which is 96% selective for the cis isomer at 423 K. Similar selectivity is observed for the other alkali-metal Y zeolites; however, the activity decreases in the order LiY > NaY ≫ KY > CsY. HY zeolites and nonzeolitic supports showed nonselective hydrogenation properties. Clearly, the catalytic efficacy of these systems is related to the cation while the selectivity can be assumed to be a function of the zeolite structure. This provides an example of how a catalytic reaction can be used to indicate intrazeolitic entrapment of the reactive species (Scheme I). IR, TPD, and ^{13}CO isotope labeling techniques indicate the active species is an anchored $Mo(CO)_3$ fragment. IR evidence also implicates an $Mo(CO)_3$(butadiene) complex as an intermediate in the hydrogenation process. Recent studies of other intrazeolite carbonyl complexes display IR spectra that are diagnostic of a cation–carbonyl interaction (described later). On the basis of these observations, a possible catalytic cycle for the intrazeolite hydrogenation of 1,3-butadiene may be proposed (Scheme 2).

In this same vein subcarbonyl moieties of iridium and rhodium have been exhaustively studied. Ion exchange of these transition-metal cations into X or Y zeolites followed by exposure to CO leads to the formation of well-characterized monovalent carbonyl species, $[M(CO)_2]^+$.[15] These zeolite-stabilized intermediates are active catalysts in the carbonylation of methanol in the presence of methyl iodide[16,17] and in the water gas shift reaction.[18] The internal entrapment of these moieties has been probed by their reactions with phosphines.[19] With small phosphines, such as $P(CH_3)_2(C_6H_5)$, $[Rh(CO)_2]^+$ in NaX reacts to form $[Rh(CO)(PMe_2Ph)_x]^+$, where x = 1, 2, or 3. By contrast, with phosphines too

large to penetrate the pore opening of the zeolite, no reaction is observed, indicating the reactive dicarbonyl is internally confined (Scheme 1).

The incorporation of carbonyl complexes within the large pores of zeolites and their intrazeolite interactions have been more fully investigated with $Fe(CO)_5$, $Fe_2(CO)_9$, $Fe_3(CO)_{12}$, $Co_2(CO)_8$, and $Ni(CO)_4$.

The interaction and intrazeolite chemistry of iron carbonyls have received much attention. In dehydrated HY, $Fe(CO)_5$, $Fe_2(CO)_9$, and $Fe_3(CO)_{12}$ are adsorbed intact with no alteration to the molecular structure.[20] Vacuum treatment of the mono- and bis-iron systems leads to the evolution of CO and formation of $Fe(CO)_4$ bonded to the zeolite while such treatment has no effect on the $Fe_3(CO)_{12}$ system. Heating to 250 °C leads to complete decarbonylation of all the carbonyl systems and oxidation of Fe^0 to Fe^{2+} ions located in the supercage. This is in contrast to a conventionally iron-exchanged zeolite where the cations locate in inaccessible sites in the sodalite cages. The $Fe_3(CO)_{12}$/NaY system provides an active catalyst for the conversion of syngas.[21]

Adsorption of $Fe(CO)_5$ into various zeolites shows a difference in the degree of interaction: dealuminated Y < CsY < HY < NaY as evidenced by the increased IR bandwidths in the CO region and the increasing intensity of the symmetric Raman-active vibration which becomes IR active,[22] attributed mainly to the electrostatic fields inside the zeolite. Thermal decomposition of this compound in various alkali-metal Y zeolites leads to iron clusters.[23] The effect of the substrate on the decomposition of $Fe(CO)_5$ has been followed by thermogravimetric measurements, IR spectroscopy, Mössbauer spectroscopy, and EXAFS.[24] In CsY, the final product is iron oxide while in NaY, zerovalent iron particles are formed.

Dicobalt octacarbonyl can be sublimed directly[25] or adsorbed from pentane solution[26] into the α-cages of X and Y zeolites. Vapor-phase impregnation into NaY, CoY, and HY has been followed in the far-IR region.[27] The vibrational frequencies of the charge-compensating cations of the zeolite occur in this region (50–350 cm^{-1}) and the band positions of the various sites have been well established. Adsorption of $Co_2(CO)_8$ into NaY and CoY causes a broadening and a shift to lower frequency of the site II cation band and a concomitant shift to higher energy of the site III band (Figure 4). A similar effect is seen for pyridine adsorbed into NaY and is believed to indicate that the compound is initially adsorbed into the supercage where it interacts with accessible supercage cations (Scheme 1). In HY zeolite new bands appear in the far-IR region. One band grows in at 150 cm^{-1} while the other appears beneath the residual Na^+ site II vibration at 185 cm^{-1} (Figure 5). The far-IR cation bands generated in this way are of the same frequencies as those of site II and III′ Co^{2+} in a cobalt ion exchanged zeolite Y. The encapsulated $Co_2(CO)_8$ has been oxidized to Co^{2+} in supercage sites II and III′ (Scheme 3). A possible mechanism consistent with the formation of the cation as well as the other carbonyl species identified by mid-IR is as follows:

$$Co_2(CO)_8 + ZOH \rightarrow \{ZOCo(CO)_4 + HCo(CO)_4\} \rightarrow$$
$$ZO\text{–}Co^{2+} + 4CO + \tfrac{1}{2}H_2 + [Co(CO)_4]^- + \{Co_4(CO)_{12}\}$$

Size-exclusion studies have been carried out with small-pore NaA zeolite. The 4-Å pore opening of this zeolite is too small to admit any larger molecules so any adsorption will occur only on the outer surface of the crystal. Exposure of NaA to $Co_2(CO)_8$ vapor under the same conditions as above shows no perturbation of the far-IR Na^+ modes. Any externally adsorbed compound has no effect on the spectrum. Therefore, it can be concluded that the changes observed in the Y zeolites are due to internal confinement of the guest molecule (Scheme 1).

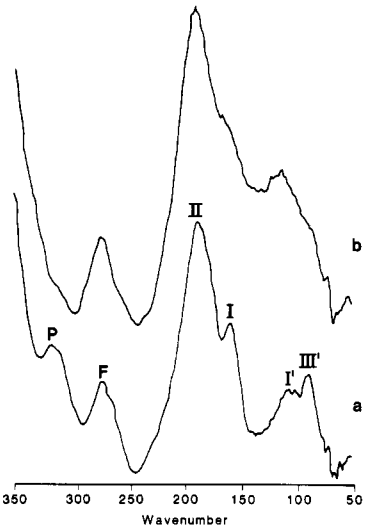

Figure 4. In situ FT-far-IR spectra of (a) vacuum thermally dehydrated $Na_{56}Y$ and (b) $Na_{56}Y$ following 15-min exposure to $Co_2(CO)_8$ vapor. Reprinted from ref 27; copyright 1986 American Chemical Society.

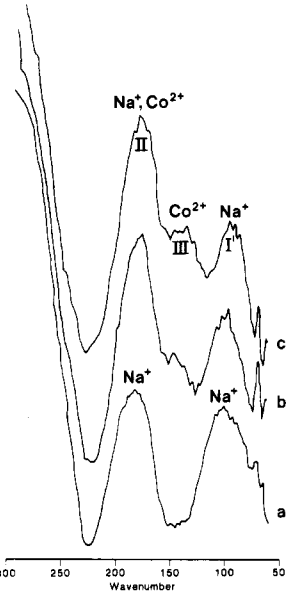

Figure 5. In situ FT-far-IR of (a) vacuum thermally dehydrated/deamminated $H_{48}Na_8Y$ showing residual sodium sites and (b, c) the outcome of exposure to $Co_2(CO)_8$ vapor for 5 and 15 min, respectively, showing the formation of Co^{2+} cations in accessible α-cage sites II and III′. Reprinted from ref 27; copyright 1986 American Chemical Society.

Changes in the mid-IR carbonyl region indicate that $Co_2(CO)_8$ reacts intrazeolitically to form the tetramer, $Co_4(CO)_{12}$, the anion, $Co(CO)_4^-$, and various subcarbonyl species in NaY as outlined above.[25,26] The location of the $Co_4(CO)_{12}$ so formed has resulted in some innovative probes for the question of internal versus external en-

SCHEME 3. Intrazeolite Organometallic Reactions with Brønsted Acid Zeolites

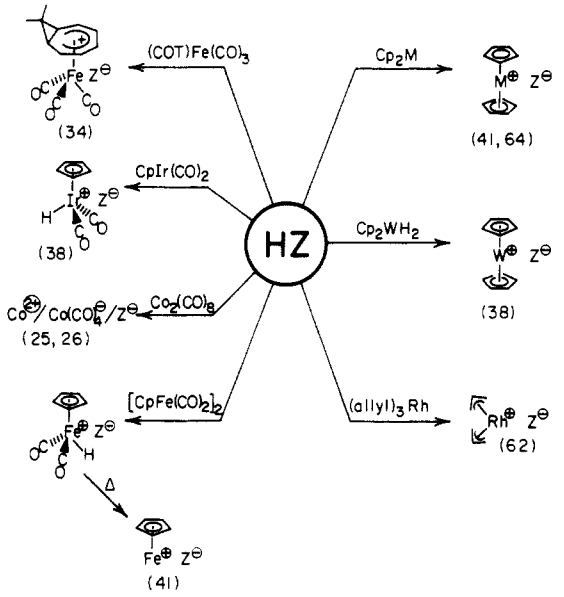

trapment of the species. The carbonyl bands observed for the tetramer formed from the $Co_2(CO)_8$/NaY system are of "higher" frequency than in solution. This shift has been attributed to an internally confined species experiencing the high electrostatic fields that exist inside the α-cage. However, adsorption of $Co_4(CO)_{12}$ onto NaY leads to CO bands at "similar" frequencies to those assigned to the tetramer formed from the $Co_2(CO)_8$/NaY system.[26] The size of the tetramer is such that it is not expected to diffuse into the large cages so it can only be physisorbed on the zeolite external surface. From these data it is believed that the cluster formed from $Co_2(CO)_8$ is therefore located on the outer surface of the zeolite.

As further evidence for these proposals the reactivity of the supported carbonyl compounds toward phosphines was investigated. With small phosphines, i.e., PEt_3, all the supported carbonyls formed from $Co_2(CO)_8$ impregnation of NaY react to form the anion, $[Co(CO)_4]^-$, the result of the disproportionation reaction involving the counterion, $[Co(PEt_3)_6]^{2+}$.[26] Such reactivity is observed for $Co_2(CO)_8$ in solution. The tetramer usually yields neutral substituted clusters in solution; however, it is apparently activated toward disproportionation on zeolites. Exposure of the same impregnated zeolite to a phosphine too large to enter the supercage, such as P^tBu_3, leads to the production of only $[Co(CO)_4]^-$. The phosphine has not penetrated the pores to react with the internally confined species but has reacted with the externally entrained species, namely, the tetramer. Therefore, the small frequency shifts observed in the $Co_4(CO)_{12}$ carbonyl spectrum are probably due to interactions with the zeolite external surface and not due to internal electrostatic field effects.

The chemistry of these supported cobalt carbonyls has been investigated with, for example, their reactivity toward NO.[28] In both NaY and NaX, conversion of $Co_2(CO)_8$ to $Co(CO)_3NO$ is observed followed quickly by the production of a trinitrosyl of cobalt assigned as $Co(NO)_3$. Direct addition of $Co(CO)_3NO$ to NaX leads to the spontaneous formation of the trinitrosyl with a concomitant production of some cobalt metal.[28]

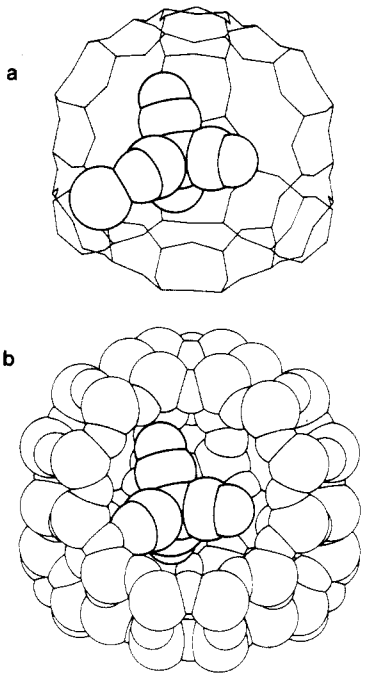

Figure 6. Model of $Ni(CO)_4$ binding to a Na^+ cation in a NaY supercage: (a) framework model; (b) model including van der Waals radii. Reprinted from ref 31; copyright 1988 American Chemical Society.

Nickel tetracarbonyl has been studied on numerous supports in order to probe the surface/support interaction[29] and subsequent decomposition pathways.[30] An interesting aspect of this work has been the recent observation of the cation dependence of the carbonyl IR spectrum.[31] In THF solution, $Ni(CO)_4$ exhibits only one CO band, consistent with its tetrahedral geometry. In dealuminated NaY only one band is observed although it is broadened due to perturbations of the molecular symmetry by the zeolite lattice. In NaY four terminal CO bands are observed. The symmetry distortion leading to the increased number of bands is thought to arise from cation–carbonyl bridges (Figure 6) similar to those observed with Al^{3+} cations on alumina[32] and with alkali-metal cations in solution.[33] In LiY, at low carbonyl loadings, a similar four-line spectrum is observed with slight frequency shifts. At high loadings only one band appears in LiY, indicative of the undistorted T_d symmetry. The increased carbonyl loading is accompanied by a decrease in the population of supercage cation sites with the lithium material. Each adsorbed molecule can no longer interact with cations but rather, most are unperturbed leading to the solution-like T_d symmetry. The same type of interaction may occur in other metal carbonyl systems. Another recently reported example concerns the intrazeolite reactivity of $(COT)Fe(CO)_3$ in NaY.[34] The IR data of the carbonyl bands provide evidence for interactions of the type $Na^+\cdots OC(CO)_2Fe(COT)$, which resembles contact ion-pair interactions of carbonyl complexes with alkali-metal cations in solution.[33] In the case of intrazeolite dicobalt octacarbonyl the IR stretching frequency of the bridging carbonyls decreases by about 30 cm^{-1} while the terminal bands increase in frequency by 10–15 cm^{-1} relative to the silica-supported material. Preferential cation interaction with bridging carbonyls is observed in solution and results in similar frequency shifts. Preferred cation interaction with bridging car-

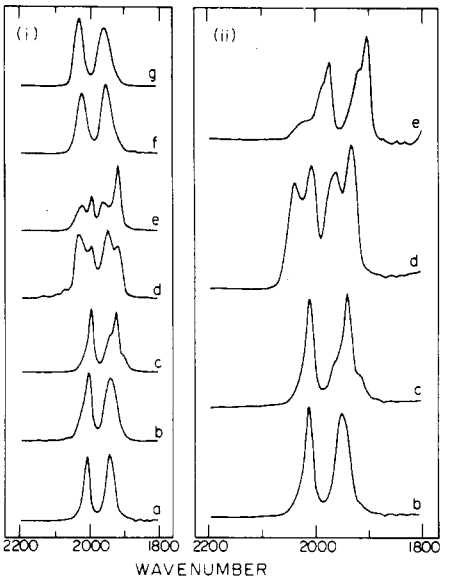

Figure 7. Cation effects on site distributions and band frequencies for (i) $CpIr(CO)_2$ and (ii) $CpRh(CO)_2$ in (a) CsY, (b) RbY, (c) KY, (d) NaY, (e) LiY, (f) NaX, and (g) NaA.[36]

bonyl ligands can be observed intrazeolitically as well.

The reactivity of the aforementioned encapsulated nickel carbonyl compound with phosphines points to the possibility of generating and trapping catalytically active organometallic species inside the zeolite pores. With phosphines small enough to enter the zeolite micropores, complexes such as $Ni(CO)_3PMe_3$ can be formed. Reaction of the encapsulated nickel carbonyl with larger phoshines can lead to the production of complexes inside the α-cages that are too large to exit the pores, for example, $Ni(CO)_3(PPh_2CHMe_2)$, the "molecular ship in a bottle" analogy (Scheme 1). Pore blocking is observed in zeolites with high initial transition-metal ion loadings. Reaction of $Ni(CO)_4$/NaY with trimethyl phosphite produces internally confined mono-, bis-, and tris-substituted complexes but a large portion of $Ni(CO)_4$ remains unreacted.[35] This is attributed to pore blocking in the higher loaded zeolites. At high nickel loadings, reaction with $P(OEt)_3$ occurs on the external surface to yield predominantly $Ni(CO)_2[P(OEt)_3]_2$. This effectively blocks the interior from the phosphite, thereby leaving unreacted $Ni(CO)_4$. At low loadings all the tetracarbonyl is consumed. XPS data confirm that reaction occurs only at the surface in the higher loaded systems. Formation of the coordinatively unsaturated $Ni(CO)_3$ intermediate in the zeolite and its reactivity clearly indicate the potential of these systems for interesting chemistry and catalysis.

(ii) Half-Sandwich Carbonyl Compounds

Recent work in our laboratory has focused attention on intrazeolite half-sandwich carbonyl compounds of iridium and rhodium. Incorporation of $CpM(CO)_2$ into NaY yields a four-band mid-IR spectrum in the terminal carbonyl region (Figure 7).[36] Attempts to sublime the compound into NaA zeolite result in only minor uptake of the organometallic as observed by the weak carbonyl stretches in the mid-IR. Using K_8Na_4A as the substrate yields even a lower degree of adsorption, and the compound is readily removed from the zeolite under dynamic vacuum in a matter of minutes. In NaY, $CpIr(CO)_2$ appears indefinitely stable and

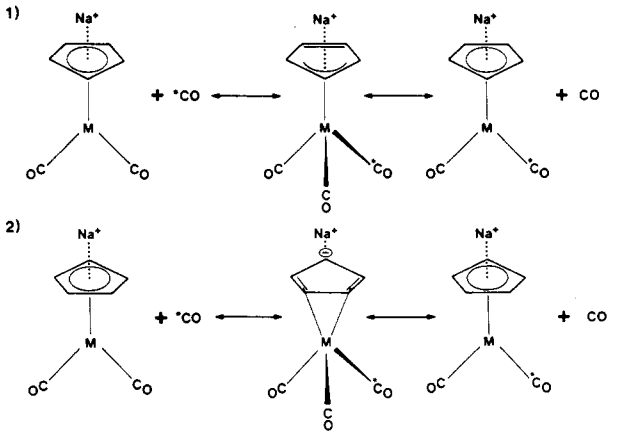

Figure 8. Intrazeolite associative ^{13}CO exchange mechanism proposed for $CpM(CO)_2$, M = Rh, Ir.[36]

cannot be removed by vacuum treatment. The pore opening of NaA is close to the dimensions of the molecule and may allow some penetration. However, the K_8Na_4A zeolite has a window opening far smaller than the guest molecule so only the externally, physisorbed organometallic is observed. The large amount of dicarbonyl adsorbed into NaY and its stability clearly indicate it is adsorbed into the internal channels of the Y zeolite where it is stabilized by interaction with the lattice (Scheme 1).

The carbonyl spectrum is therefore attributed to two different types of interactions within the α-cage. A cation–carbonyl interaction similar to that observed for $Ni(CO)_4$ is assigned to the strongly red shifted site, designated site 2. The roughly 50-cm^{-1} shift from solution-phase values is consistent with such an interaction. The second set of CO bands, attributed to a solution-like species and designated site 1, may simply represent a nonspecific weakly interacting molecule confined inside an α-cage. Alternatively, it may involve a cation–ring interaction as previously observed for aromatic hydrocarbons in zeolites.[37] Similar perturbations are observed for $Cp^*M(CO)_2$ complexes in the Y zeolites. Incidently, reaction of $CpIr(CO)_2$ with $H_8Na_{48}Y$ yields the intrazeolite protonated form, $[CpIr(CO)_2H]^+$ (Scheme 3).[38] The cation dependence of the band positions and population distributions for both sites also attests to an internally confined compound interacting with cations (Scheme 1). The ring interaction is believed to stabilize the intermediate in the observed associative ^{13}CO exchange reaction (Figure 8). In NaY, ^{13}CO exchange is instantaneous at room temperature while it does not occur in solution in the absence of light.[39] The fastest ^{13}CO exchange rates are observed when both sites are at least partially occupied. With $CpM(C_2H_4)_2$ as the precursor molecule, enhanced CO substitution rates are also observed. While these compounds are inert to CO substitution in solution at room temperature,[40] they undergo rapid exchange in NaY. Again stabilization of the intermediate via cation–ring interaction may be responsible for this rate enhancement.

Vacuum thermal treatment of these intrazeolite dicarbonyls leads to gradual loss of CO. In the case of $CpIr(CO)_2$ in NaY there appears to be an initial redistribution from site 2 to site 1 dicarbonyl at low temperatures, ca. 150 °C, followed by complete decarbonylation by 300 °C. The rhodium analogue, CpRh-

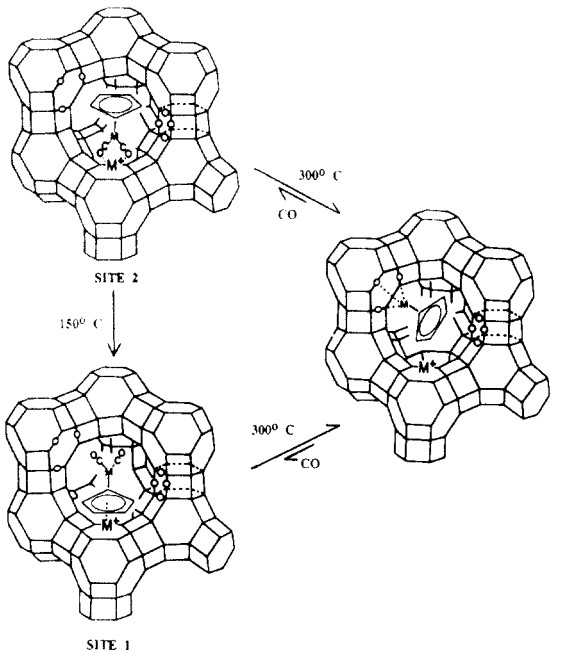

Figure 9. Effect of thermolysis on $CpM(CO)_2$ in NaY. Apparent site interconversion occurs for M = Ir at 150 °C, while the half-sandwich, CpIr, is formed at higher temperatures. For M = Rh the half-sandwich is formed at lower temperatures.[36]

$(CO)_2$, shows no initial redistribution but a faster loss of site 2 dicarbonyl relative to site 1. Retention of the ring C–H modes after complete decarbonylation is indicative of the formation of the half-sandwich, CpM (Figure 9). These half-sandwiches may also be generated by thermolysis of the bis(ethylene) precursors, $CpM(C_2H_4)_2$. Although the intrazeolite iridium half-sandwich is fairly inert, intrazeolite CpRh gives about a 50% back-reaction to $CpRh(CO)_2$ upon exposure to CO at room temperature in the same site distributions initially observed. The catalytic potential of such unsaturated intermediates is immediately clear.

In this context it is worth documenting similar intrazeolite transformations that have been proposed to yield half-sandwich organometallic fragments. Bein et al. have studied the intrazeolite chemistry of $(COT)Fe(CO)_3$[34] and $[CpFe(CO)_2]_2$[41] with acid zeolites and found the following reactions:

$$(COT)Fe(CO)_3 + HZ \rightarrow [H(COT)Fe(CO)_3]^+Z$$

$$[CpFe(CO)_2]_2 + HZ \rightarrow [CpFe(CO)_2]_2H^+Z \rightarrow [CpFe(CO)_3]^+Z$$

The cationic complexes are thought to be stabilized by electrostatic interaction with the anionic intrazeolite oxygen surface. This process has been shown to represent the initial step of an "anchoring" sequence which is completed on heat treatment by substitution of the less stable carbonyls with zeolite oxygen ligands:

$$[H(COT)Fe(CO)_3]^+Z \rightarrow [H(COT)Fe]^+Z$$

$$[CpFe(CO)_3]^+Z \rightarrow [CpFe]^+Z$$

In this way zeolite-anchored half-sandwich fragments remain and represent potential reactive centers in the zeolite cage. These studies form a sound basis for the development of well-defined hybrid catalysts based on zeolite hosts. Incidently, the intrazeolite protonation of $(COT)Fe(CO)_3$ described above is thought to lead to the (bicyclo[5.1.0]octadienyl)iron tricarbonyl cation in a clean reaction, which corresponds to the protonation of $(COT)Fe(CO)_3$ with noncoordinating acids like HBF_4 in homogeneous solution.

Studies of the interaction of metal carbonyls with zeolites have progressed rapidly. Although viable as precursors for the formation of intrazeolite metal particles, they have clearly also demonstrated unique anchoring effects and chemistry within the zeolite lattice. The increased possibilities this represents leave much to be investigated.

D. Coordination Compounds

(i) Weak Complexes

Many coordination complexes can be formed within zeolite pores by simple reaction of the exchanged metal cations with various organic molecules. Some of these so-formed species are not very stable and can be destroyed by evacuation or gentle heating. Nonetheless they do attest to the possibility of forming and characterizing internally confined coordinately saturated and unsaturated coordination complexes.

Copper-Y zeolite reacts with alkynes, C_2H_2, C_3H_4, and C_2D_2 to give a copper ion–alkyne bond resulting mainly from π donation from the unsaturated hydrocarbon to the metal cation.[42] Ethylene is strongly bound to Cu^IY and Ag^IY zeolites at room temperature but not to $Cu^{II}Y$, $Ca^{II}Y$, or $Zn^{II}Y$.[43] More recently, ethylene and dihydrogen complexes have been formed in Ni^+CaX.[44] Partial exchange of a CaY zeolite with nickel leads to Ni^{2+} in accessible supercage sites. Reduction with dihydrogen leads to two species identified as $Ni^+(H_2)$ and $Ni^+(H_2)_n$, n = 2 or 3, located in the supercage. These complexes are eradicated by vacuum treatment, consistent with weak complex formation. Similarly, weak Ni^+ complexes of H_2O, CH_3OH, and NH_3 have been generated intrazeolitically. The EPR of the methanol and water complexes indicates an octahedral geometry with lattice oxygen atoms occupying three sites while the amine complex is square planar with two lattice oxygen coordination sites. For $Ni^+(C_2H_4)$ and $Ni^+(CH_2CHCH_3)$ reversed g values are obtained, most likely indicating a compressed tetrahedral or square-pyramidal geometry.

Cobalt and manganese ions in partially exchanged zeolites react with cyclopropane to produce a loosely bound $M–C_3H_6$ moiety.[45] Crystal structure analysis shows the cations are located on the threefold axis inside the large cavity close to the three trigonally arranged framework oxide ions on alternate six-rings (Figure 10). No interaction is observed with residual sodium cations.

Among the first characterized coordination compounds formed intrazeolitically were the penta- and hexamethyl isocyanide complexes of cobalt.[46] Exposure of a dehydrated sample of CoCaY to excess CH_3NC at room temperature gives a product that exhibits a hyperfine octet due to ^{59}Co (Figure 11a). The EPR parameters are in close agreement with those for hexacoordinate Co(II) in D_{4h} symmetry. Partial desorption of CH_3NC yields an EPR spectrum indicative of a pentacoordinate isocyanide complex with the sixth coordination site being a zeolite lattice oxygen (Figure 11b).

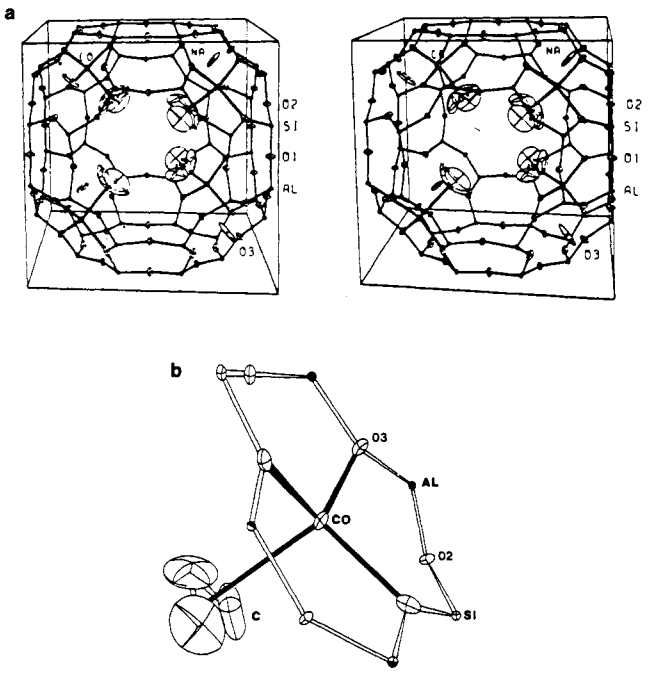

Figure 10. Intrazeolite cyclopropane complex of Co(II) in zeolite A. (a) Stereoview of the $Co_4Na_4A{\cdot}4C_3H_6$ unit cell. (b) Coordination environment of the Co(II) ion. Reprinted from ref 45; copyright 1978 American Chemical Society.

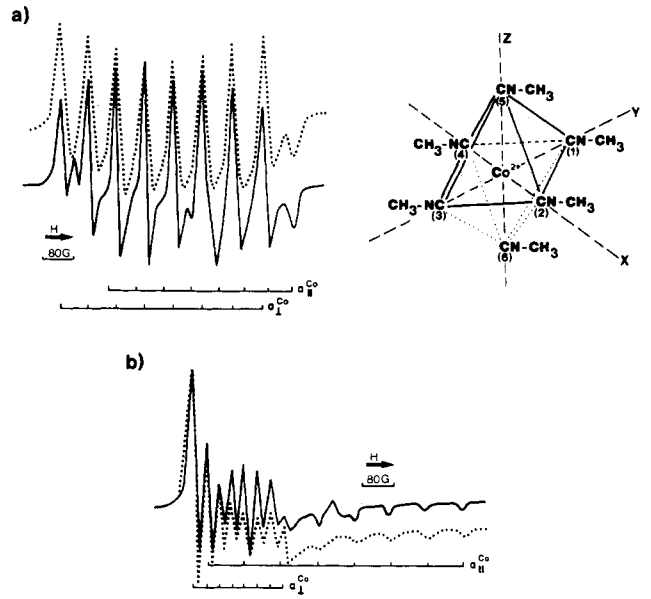

Figure 11. Intrazeolite cobalt(II)–methyl isocyanide complexes. (a) Experimental (—) and simulated (···) EPR spectra of $[Co(CH_3N^{12}C)_6]^{2+}$. (b) Experimental (—) and simulated (···) EPR spectra of $[Co(CH_3N^{12}C)_5]^{2+}$. Reprinted from ref 46; copyright 1975 Marcel Dekker.

(ii) Ethylenediamine and Pyridine Complexes

Ethylenediamine and pyridine complexes can be isolated within zeolites by direct exchange of the complex or formed by exposure of the metal ion exchanged zeolite to the ligand either in the vapor or in solution phase. The products formed vary with the zeolite, the metal center, and the method. Since little of this work has focused on the location of the coordination complex, only a brief outline will be presented.

For copper in X and Y zeolites the predominant species isolated are $[Cu(en)_2]^{2+}$ and $[Cu(en)]^{2+}$.[47,48] The $Cu^{II}(en)/Y$ system is catalytically active in the decomposition of hydrogen peroxide.[47] Exposure of an $[Ir(NH_3)_6]^{3+}$-exchanged X zeolite to ethylenediammine produces $[Ir(en)_2(NH_3)_2]^{3+}$, which is active in the water gas shift reaction.[49] Finally, CoX and CoY form predominantly $[Co(en)_2]^{2+}$ upon exposure to the ligand.[50] This species readily reacts to bind oxygen to form $[Co(en)_2O_2]^+$ as seen by changes in the EPR spectrum.

Tetrakis(pyridine)copper(II) complexes have been formed in both X and Y zeolites by simple adsorption of the ligand into the transition-metal-exchanged zeolite.[51] Reflectance spectra and EPR measurements clearly identify the species as $[Cu(py)_4]^{2+}$. In this case no mono, bis, or tris complexes are formed, in contrast to the ethylenediamine case discussed previously. The copper(II) bipyridine complex has also been observed in zeolite Y.[52] Initial ion exchange with 2,2′-bipyridinium chloride formed the bipyridinium zeolite, which was then exchanged with $^{63}Cu^{2+}$ ions. The EPR spectrum shows a five-line superhyperfine splitting pattern attributed to two equivalent nitrogen atoms, indicating the formation of $[Cu(bpy)]^{2+}$. By contrast, $Fe^{II}Y$ zeolites exposed to 2,2′-bipyridine preferentially form the tris(bipyridine)iron(II) complex characterized by Mössbauer, EPR, and reflectance techniques.[53] Subsequent exposure of this sample to chlorine gas yields the trivalent complex $[Fe(bpy)_3]^{3+}$ in 89% yield. For the tris(2,2′-bipyridine)cobalt(II) complex in zeolite Y an interesting spin equilibrium is observed.[54] At 77 K an eight-line EPR spectrum was observed with g values close to those observed for a frozen DMSO solution of $CoCl_2$ and bipyridine. This is attributed to the low-spin complex. As the temperature is increased the EPR spectrum of the low-spin complex gradually disappears. The high-spin state of the complex becomes dominant. A short relaxation time is believed to be responsible for the lack of an EPR signal.

(iii) Oxygen Carriers

Terpyridine and bipyridine cobalt complexes have been studied and yield viable oxygen carriers. Low- and high-spin $[Co(terpy)_2]^{2+}$ and five-coordinate $[Co(bpy)(terpy)]^{2+}$ can be formed in varying concentrations in CoNaY zeolite.[55] Evidence for the internal entrapment of the species was obtained by slurrying a zeolite containing the mixed complex with a benzene solution of DPPH. The DPPH is too large to enter the supercage so it would be expected to remain on the external surface of the lattice. If the two compounds interacted one would expect to see a spin-exchange effect. Following the benzene treatment, the EPR remained unchanged, indicating the complex was not in close proximity to the DPPH; that is, the complex was internally confined while the DPPH probe was on the outer surface. Exposure to oxygen results in the formation of the O_2 adduct for the mixed complex, $[Co(bpy)(terpy)O_2]^+$, but not for $[Co(terpy)_2]^{2+}$. The EPR spectrum was consistent with a bent $Co–O_2$ structure for the superoxide ion. The formation of the oxygen adduct is completely reversible at 298 K while the adduct itself is thermally stable in oxygen up to 343 K. A substantial increase in the initial concentration of the mixed complex $[Co(bpy)(terpy)]^{2+}$, can be obtained in partially cobalt-exchanged LiY at a reaction temperature of 703 K for 2 h.[56] This system is very efficient in separating O_2 from N_2 in dry air.

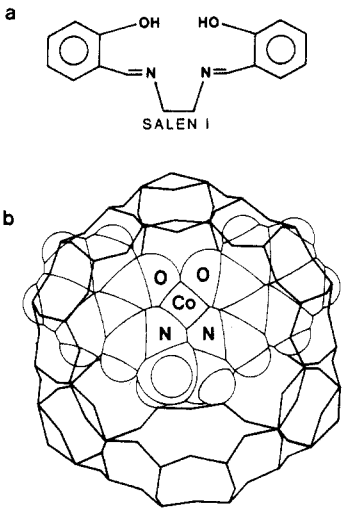

Figure 12. Pictorial representation of the Co(salen) adduct inside the supercage of zeolite Y. Reprinted from ref 57; copyright 1986 American Chemical Society.

The formation of these internal dioxygen complexes has led to the investigation of more systems for gas separation. Such complexes form in solution; however, they slowly decompose as the oxygen either attacks the ligands or the complex deactivates intramolecularly. The intrazeolite isolation and stabilization of complexes with ligands robust enough to withstand oxidation may overcome the deactivation problems of solution work.

One approach is the use of the Schiff base salen.[57] Treatment of cobalt-exchanged Y zeolite with excess Schiff base in an inert atmosphere results in the formation of the Co(salen) complex within the α-cage (Figure 12), identified by a reflectance spectrum almost identical with that of the complex in solution. Following this treatment the ligand is nonextractable, also consistent with complex formation. Size-exclusion studies with A zeolites indicate the complex is internally confined in the Y zeolites (Scheme 1). In addition, ESCA studies show very low concentrations of cobalt in the outer 50 Å of the crystallites, again in accordance with internal loading (Scheme 1). The pyridine adduct of this complex shows an affinity for oxygen. The EPR spectrum corresponds to the Co(salen)(py)(O_2) complex. In solution the peroxo dimer forms, which deactivates the catalyst. This is precluded in the zeolite. In addition, the intrazeolite complex is resistant to autoxidation even at elevated temperatures. The oxygen adduct can be dissociated simply by evacuation. Cycling between oxygenated and deoxygenated species may continue for many hours.

Recently, an anionic cobalt cyanide complex has been formed in zeolite Y[58] by slurrying a CoY zeolite with a methanolic sodium cyanide solution. (Note that, intrazeolite anion formation is most unusual. Presumably the process occurs via a salt-inclusion reaction.[2]) Exposure to oxygen results in the formation of a Co–O_2 adduct characterized by IR and EPR spectroscopy. The EPR spectrum of the deoxygenated sample is significantly different from that of the O_2 adduct (Figure 13). The g values of the deoxygenated species differ significantly from those of a five-coordinate Co(II) complex but are closer to those of a four-coordinate Co(II) complex. The large **g** tensor anisotropy is consistent with a square-planar $[Co(CN)_4]^{2-}$ complex with an axial position occupied by a framework oxygen. This zeolite

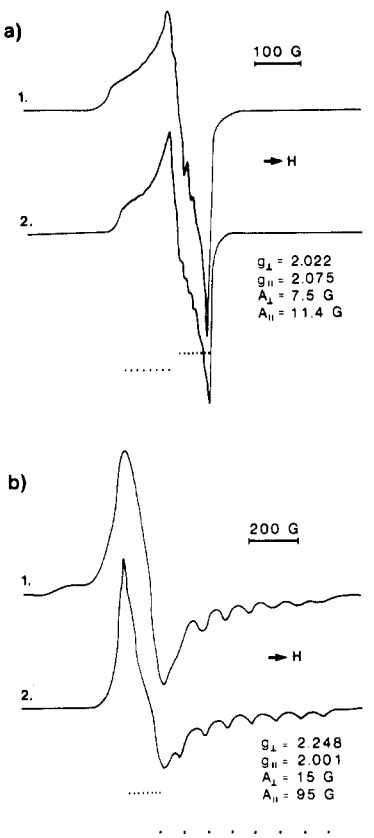

Figure 13. X-Band EPR spectra of (a) $[Co(CN)_4(O_2)]^{2-}$Y and (b) $[Co(CN)_4]^{2-}$Y [(1) experimental and (2) simulated]. Reprinted from ref 58; copyright 1988 American Chemical Society.

sample can be alternately oxygenated and partially deoxygenated at room temperature through 510 cycles over a period of 6 weeks after which the IR and EPR spectra show no sign of chemical decomposition.

(iv) Phthalocyanine Complexes

A class of very stable and well-characterized intrazeolite organometallics are the phthalocyanine complexes of transition metals. Reaction of transition metal ion exchanged X zeolites with 1,2-dicyanobenzene at 523 K results in phthalocyanine formation and complexation for the cobalt, nickel, and copper zeolites.[59] Scanning electron microscopy indicates that material formed on the external surface of the zeolite is easily removed by Sohxlet extraction (Scheme 1). Once formed, the internally confined species are too large to be extracted. The fraction of encaged phthalocyanine is determined by photometry of a sulfuric acid solution of the reacted zeolites and ranges from 22% for CoX to 4% for CuX. X-ray diffraction shows the lattice structure is largely maintained throughout the chemical procedures, and high N_2 uptake indicates only minor clogging of the internal surface.

Work by Herron and co-workers using zeolite-encapsulated iron phthalocyanine has focused on the catalytic applications of these materials.[60a] Reflectance spectra consistent with complex formation, X-ray powder diffraction patterns confirming the crystallinity of the zeolite, XPS showing no detectable surface iron, and the reduced sorption capacity of the zeolite for water are all in accordance with the formation of the FePc complex inside the supercage of the faujasite lattice (Figure 14, Scheme 1). Analytical data are in

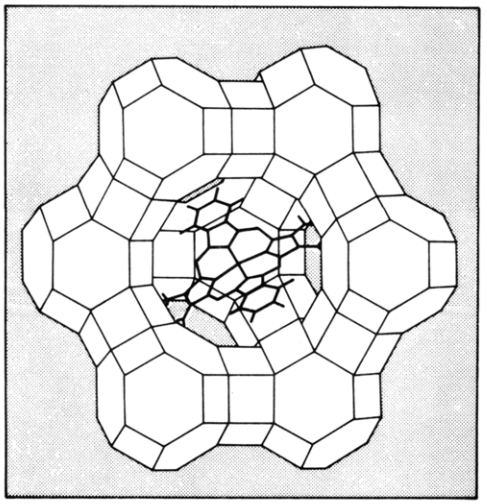

Figure 14. Intrazeolite phthalocyanine complex formation. Reprinted from *Chemical and Engineering News*, Sept 17, 1984, p 30; copyright 1984 American Chemical Society.

good agreement with the calculated Fe:C:N ratios for complete conversion of all iron to FePc. The expected shape selectivity is observed in the oxidation of alkanes with iodosobenzene in the presence of this catalyst. Competitive oxidation between cyclohexane and cyclodecane shows a preference for the smaller alkane. Regioselectivity is also seen with increased oxidation at the 2-position relative to the 4-position in *n*-octane. Finally, some stereoselectivity is also observed in the oxidation of methylcyclohexane where the trans to cis ratio is close to 2. The turnover rate for the low-loading iron zeolites is greater than for FePc itself due to the increased lifetime of the catalyst. The zeolite lattice prevents the usual bimolecular self-destruction mechanism. Although the rates are slow, the increased yields and selectivities deserve further investigation.

Coordination complexes can be readily formed or exchanged into large-pore zeolites. Some of the work presented herein clearly demonstrates quantitative internal confinement of the guest. The potential of these systems for gas separation and catalytic applications certainly warrants further study. In a fascinating recent article Herron[60b] contemplates zeolites as enzyme mimics and presents a thought-provoking case for Si-based life as well as extensions to the Si-based brain.

E. Organometallics

The ability to quantitatively locate organometallic compounds and fragments within zeolite pores creates the possibility of trapping/encaging potentially reactive species within a molecular sieve network. Much research has recently been produced that focuses on the internal/external trapping of the organometallic as well as its interactions with the lattice, resulting in some novel applications of these systems.

(i) Novel Anchoring Mechanisms

Reaction of planar bis(dithiophosphato)nickel complexes with NaX or noncalcined $Na(NH_4)Y$ results in the irreversible adsorption of the species.[61] The same complexes are not adsorbed into HiSil 233 silica gel. Internal confinement of the organometallics is confirmed by several observations. Size-exclusion studies

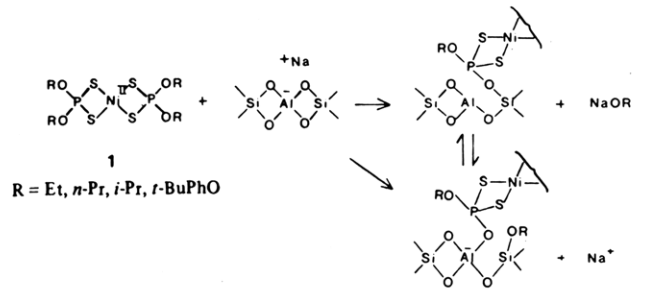

Figure 15. Proposed intrazeolite anchoring scheme for bis(dialkyl dithiophosphato)nickel(II). Reprinted from ref 61; copyright 1983 American Chemical Society.

with NaA zeolite indicate only trace adsorption of the nickel species. This is consistent with the small pore diameter of the A zeolite, which prevents entry of the large complex. X-ray diffraction indicates an increase in the unit cell size and shows large losses of signal intensity in reflections that are influenced by intracage perturbations. Both observations are consistent with an encaged complex interacting with the lattice. Reaction of this system with 1 N NaOH at 90 °C strips most of the nickel from the zeolite, and the X-ray parameters return to their normal values. Finally, an upper limit of 1.59% nickel is adsorbed by NaX when the Ni:zeolite ratio is varied, corresponding to 0.5 nickel atom per supercage. Only enough complex is adsorbed to fill the zeolite pores. If the complex were externally held, continuous adsorption would be expected to some large upper limit.

Interaction of the complex with zeolite Brønsted acid sites is discounted since little alcohol production from the anchoring reaction is observed by gas chromatography:

$$ZOH + [(RO)_2PS_2]_2Ni \rightarrow ZOP(OR)S_2Ni[(RO)_2PS_2] + ROH$$

A more likely interaction is thought to occur with basic AlO_4^- sites through a phosphonium-like intermediate (Figure 15). FTIR diffuse reflectance ratio spectra show differences in the regions assignable to P–S and P–O stretching modes. A band at 886 cm^{-1} can be reasonably assigned to a P–O–T (T = Si or Al) stretching vibration, which is consistent with the proposed anchoring linkage. Although the intrazeolite complex exhibits increased thermal stability, it is deactivated toward adduct formation with, for example, primary amines. Nonetheless this demonstrates a novel internal anchoring mechanism and shows several methods for locating the organometallic compound.

The anchoring and catalytic potential of intrazeolite organometallics is demonstrated by Schwartz's tris(π-allyl)rhodium.[62] Reaction of this complex with a partially proton-exchanged NaX zeolite leads to the loss of one propylene group, determined by GC/MS, leaving the bis(π-allyl)rhodium fragment bonded to a lattice oxygen through the metal center (Figure 16a, Scheme 3). Hydrogen treatment results in the formation of the allyl hydride, which shows high catalytic activity for olefin hydrogenation. Unlike the silica-supported analogue, the zeolite system shows size/shape selectivity for the substrate. This is attributed to the molecular discriminating nature of the zeolite lattice (Figure 16b) and indicates the catalytic species is internally confined (Scheme 1). Although a linear uptake of H_2 was ob-

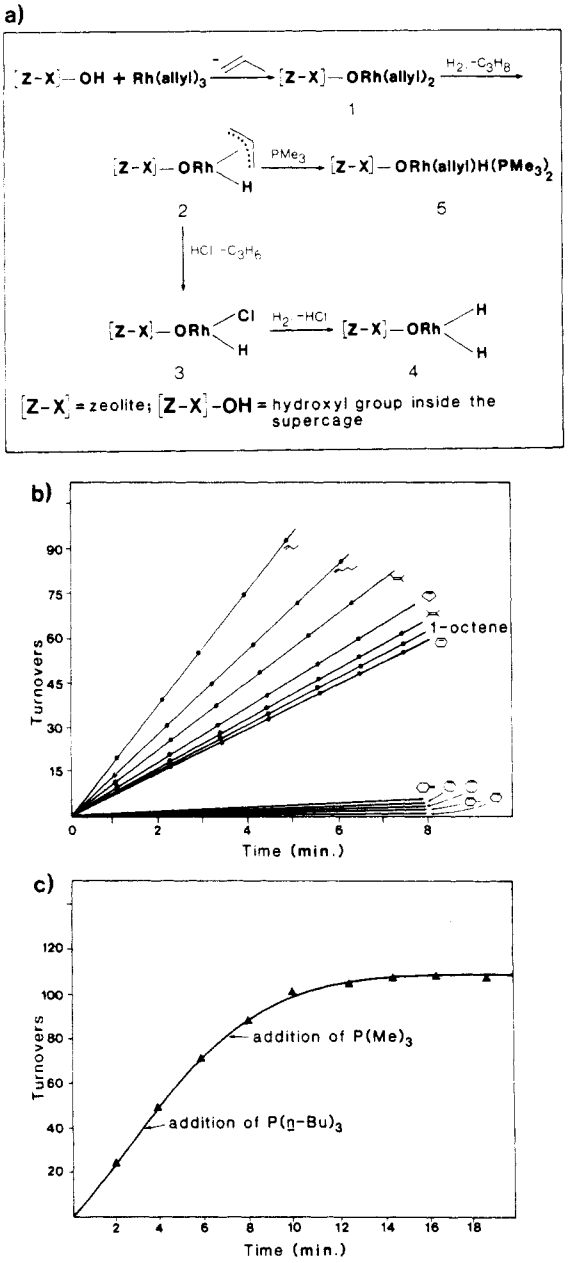

Figure 16. Intrazeolite $Rh(allyl)_3$: (a) Anchoring mechanism and chemical reactivity; (b) rate of hydrogenation of olefins catalyzed by (Z-X)-ORh(allyl)H; (c) hydrogenation of 1-butene by (Z-X)-ORh(allyl)H followed by sequential additions of PBu_3 and PMe_3. Reprinted from ref 62; copyright 1982 American Chemical Society.

served for all olefins studied, the rates of hydrogenation of substrates larger than cyclohexene were negligible. These larger molecules are unable to pass through the zeolite channels to the catalytically reactive center. Shape selectivity is observed in the rapid hydrogenation of benzene compared to the slow reaction of toluene under identical conditions. To further prove the contention of an internal complex, selective poisoning experiments with phosphines of varying sizes were carried out (Figure 16c, Scheme 1). Addition of PBu_3 to the reaction mixture does not significantly alter the rate of hydrogenation of 1-butene. However, addition of the much smaller PMe_3 causes the rate to drop almost immediately to zero. This phosphine is able to penetrate the zeolite pores and coordinate with the complex, thereby poisoning it to further catalysis. The larger

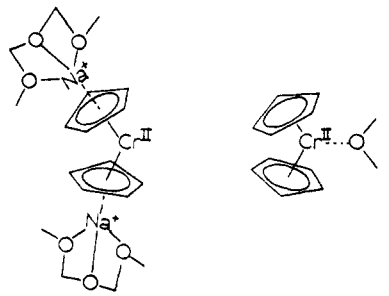

Figure 17. Intrazeolite trapping schemes envisaged for Cp_2Cr. Reprinted from ref 64; copyright 1989 American Chemical Society.

PBu_3 is unable to enter the pores and so has no effect on the hydrogenation rate. In a following study using competitive hydrogenation of cyclopentene and 3- or 4-methylcyclohexene, a greater selectivity in the hydrogenation of olefins is observed for zeolites that are ion exchanged with rhodium cations than for the Schwartz system.[63] Selectivity requires poisoning of external metal sites with bulky phosphines and varies with the zeolite used as well as its water content. Nonetheless, Schwartz's approach may provide a general method for incorporating organometallic complexes into the supercages of X and Y zeolites. In addition, mild activation procedures minimize degradation of the catalytic species and avoid the metal clustering/sintering problems encountered in previous work.

(ii) Metallocenes

Metallocenes are easily exchanged into zeolites and conveniently studied by a variety of spectroscopic techniques. Unique interactions with the zeolite lattice have been observed. Godber and Ozin have used these sandwich compounds and their derivatives to investigate internal versus external confinement of the guest molecule and the homogeneity of impregnation.[27,64] Using optical reflectance, vibrational and paramagnetic resonance spectroscopies, Godber and Ozin have observed both ferrocene and chromocene to readily diffuse into large-pore zeolites.

With Cp_2Cr as an EPR spin probe the external/internal confinement of the guest can be investigated with a size-exclusion experiment. The dimensions of this molecule are such that it can enter the pores of X and Y zeolites but is precluded from entering the A zeolites. Following solution-phase impregnation of Cp_2Cr into several zeolites, EPR spectra show distinct differences. In 2-methyltetrahydrofuran, at 100–120 K, chromocene exhibits an EPR spectrum indicative of a distorted molecule with a triplet ground state: $g_\perp = 2.012$; $g_\parallel = 1.988$. On NaA only very weak EPR resonances are observed which are attributed to residual externally confined Cp_2Cr. In $Na_{56}Y$, Cp_2Cr displays a temperature-dependent EPR spectrum. At room temperature a spectrum characteristic of a rhombic distortion from pseudoaxial symmetry is obtained ($g_\perp = 2.160$; $g_\parallel = 2.058$) which is associated with the triplet ground state. At 123 K a parallel-like feature with $g_\parallel = 4.001$–4.026 appears concomitant with a shift of the high-field resonances to $g_\perp = 2.252$ and $g_\parallel = 2.063$. The new signal is associated with the doublet ground state of Cp_2Cr made available by the increased distortion imposed by the zeolite lattice. This indicates that the complex is immobilized in the supercage of NaY in a distorted

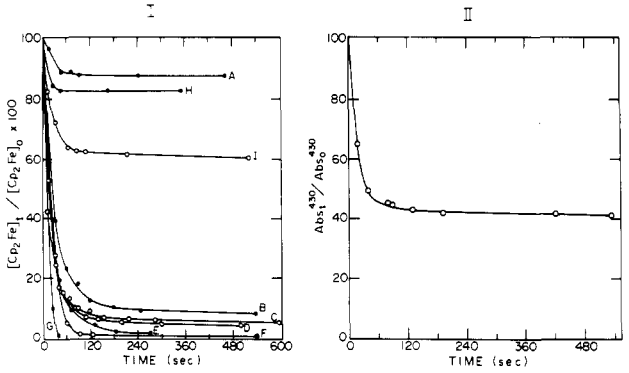

Figure 18. (I) Normalized absorbance plots of the impregnation rates of (A) $Cp^*_2Fe/Na_{56}Y$(D), (B) $Cp_2Fe/Na_{56}Y$, (C) $Cp_2Fe/H_{16}Y$, (D) $Cp_2Fe/[HPMe_3]_8Y$, (E) Cp_2Fe/NaY(D), (F) Cp_2Fe/H_8Y, (G) $Cp^b_2Fe/H_{56}Y$, (H) Cp_2Fe/SiO_2-500, and (I) $Cp_2Fe/Ca_{28}Y$ (where $Na_{56}Y$(D) refers to a defect removed sodium Y zeolite that has been rigorously dehydrated/calcined and CH_3Li treated). (II) Normalized absorbance plots of the impregnation rate of an equimolar mixture of $Cp^*_2Fe/Cp_2Fe/H_{16}Y$. Reprinted from ref 64; copyright 1989 American Chemical Society.

configuration induced by either cation or framework oxygen atoms (Figure 17, Scheme 1). In $H_{48}Na_8Y$ chromocene is oxidized and anchored as Cp_2Cr^+ as seen by diagnostic changes in the EPR spectra. Clearly, the metallocene is unhindered from entering zeolites with window dimensions large enough to admit it (Schemes 1 and 3).[27,64]

The diffusion of ferrocene from pentane solution into several dehydrated zeolites was followed by quantitative UV–vis spectroscopy.[27,64] The change in concentration of the organometallic in solution as a function of time indicates that within 3 min >90% of the compound is adsorbed into the zeolite (Figure 18). This is consistent with its unconstrained diffusion into the zeolite pores. It should be noted that Cp_2Fe is excluded from non-dehydrated or partially dehydrated NaY due to pore blocking by water molecules. Conversely, the larger Cp^*_2Fe is size excluded from entering the faujasite lattice. The small uptake of Cp^*_2Fe corresponds to that restricted to the outer surface of the zeolite. This is consistent with the amount of Cp_2Fe adsorbed from solution onto SiO_2 dehydrated at 500 °C. In addition, competitive diffusion between an equimolar mixture of Cp_2Fe and Cp^*_2Fe into NaY suggests that Cp_2Fe readily diffuses into the zeolite while the bulkier compound remains largely in solution.

Ferrocene uptake by acid zeolites provides a means of probing the homogeneity of the organometallic distribution within the zeolite crystals.[64] In NaY ferrocene exhibits a low symmetry distortion, similar to chromocene, as indicated by the appearance of Raman-active modes in the mid-IR. In acid zeolites oxidation occurs to Cp_2Fe^+, also similar to the chromocene system (Scheme 3). This is readily observed in the optical reflectance and EPR spectra of ferrocene. After impregnation into $H_{48}Na_8Y$ only bands attributable to ferricinium are observed, with a complete absence of ferrocene absorptions. Oxidation of Cp_2Fe to Cp_2Fe^+ in HY occurs concurrently with a loss of α-cage hydroxyl groups. These protons are homogeneously distributed throughout the zeolite lattice. The complete uptake of known amounts of these protons upon exposure to stoichiometric quantities of the organometallic is indicative of an even distribution of the

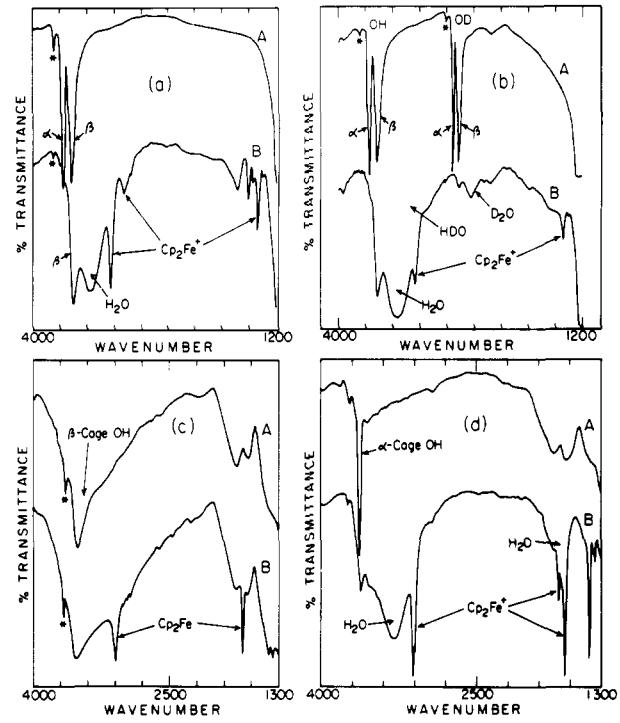

Figure 19. (a) In situ mid-IR spectra of (A) vacuum thermally dehydrated zeolite Y and (B) the outcome of impregnation by gaseous Cp_2Fe. (b) In situ mid-IR spectra of (A) vacuum thermally dehydrated $H_{28}D_{28}Y$ and (B) the outcome of impregnation by gaseous Cp_2Fe. (c) In situ mid-IR spectra of (A) vacuum thermally dehydrated $Cs_{36}H_{20}Y$ and (B) the outcome of impregnation by gaseous Cp_2Fe. (d) In situ mid-IR spectra of (A) thermally dehydrated H_8Y and (B) the outcome of impregnation by gaseous Cp_2Fe. The asterisk denotes a small concentration of OH groups on the external surface of the zeolite crystals. Reprinted from ref 64; copyright 1989 American Chemical Society.

complex throughout the zeolite crystals (Figure 19). The mechanism of this process has been extensively studied by using isotopically H/D-labeled zeolites. The results indicate α-cage Brønsted acid site-specific electron transfer, redox-induced H atom/lattice OH radical production of H_2O, and concurrent production of Cp_2M^+ with three-coordinate Al and Si framework radical centers.[64]

Thermal treatment of $[Cp_2Fe]^+Z$–Y has recently been demonstrated to lead to the zeolite-anchored half-sandwich complex $[CpFe]^+Z$–Y,[41] comparable to the reaction that anchors a $[CpFe]^+$ fragment into zeolite cages upon thermal decomposition of $[CpFe(CO)_2]_2$ in acid zeolite Y.[41] These studies illustrate that organometallic iron compounds are well suited for anchoring organoiron fragments to specific binding sites in molecular sieve supports by establishing a stable bond to the ring-shaped oxygen coordination sites in the cage system.

The cationic sandwich complexes can be formed within the zeolite pores or simply exchanged for charge-balancing cations. Controlled O_2 oxidation of intrazeolite Cp_2Cr leads to spatially and charge-separated cation/anion pairs, Cp_2Cr^+/O_2^- (Figure 20).[64] Aqueous ion exchange of Cp_2Co^+ into KY, CaY, and LaY shows a high level of exchange, 1 Cp_2Co^+/unit cell in KY and up to 4/unit cell in CaY and LaY.[65] The resonance Raman spectra of the intrazeolite metallocene are of better quality than those in solution. In the mid-IR the C–H stretching mode of the Cp ring shifts to lower frequency. The metal–ring stretch and ring

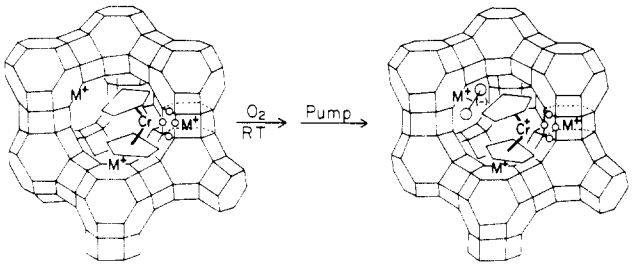

Figure 20. Intrazeolite oxidation of Cp_2Cr resulting in spatially and charge-separated cation/anion pairs, Cp_2Cr^+/O_2^-. Reprinted from ref 64; copyright 1989 American Chemical Society.

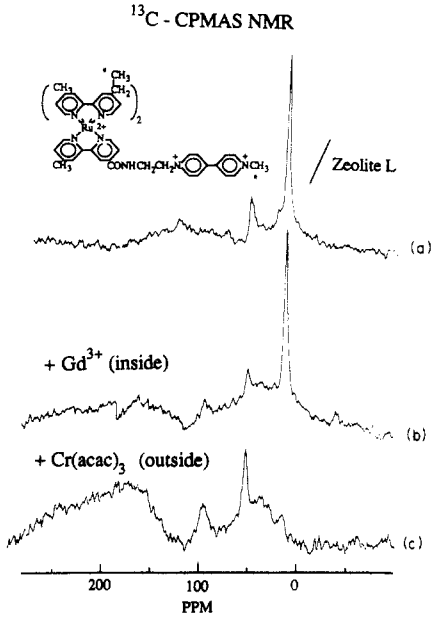

Figure 21. ^{13}C CPMAS NMR of linked $[Ru(bpy)_3]^{2+}$–viologen^{2+} (a) in zeolite L (b) + Gd^{3+} (inside) (c) + $Cr(acac)_3$ (outside).[66]

breathing modes also become weaker down the series KY > CaY > LaY. Increased polarization within the zeolite makes the intrazeolite water molecules better H-bond acceptors from the Cp ring. This leads to a higher positive charge on the metal and excess negative charge on the ring. Upon dehydration the ring breathing mode red shifts, approaching 983 cm^{-1}, the value for the free cyclopentadienyl anion.

(iii) Molecular Microstructures

Recently, zeolites have been used to create supramolecular organized assemblies of redox-active guests. Redox-active species can be preferentially located both internally and externally by using large-pore zeolites. Although physically separated, the molecules are still in close enough proximity to, for example, act as electron relays.

The ability to preferentially locate some molecules intrazeolitically while anchoring others on the external surface is demonstrated by using a linked $[Ru(bpy)_3]^{2+}$–viologen^{2+} complex with ^{13}C labels at either end and ^{13}C CPMAS NMR as a diagnostic probe[66] (Scheme 1). This complex was exchanged into a partially dehydrated zeolite L to a concentration of 1×10^{-5} mol/g. Peaks were observed at +10 and +50 ppm due to the labeled methyl groups on the 2,2′-bipyridine group and on the quaternary nitrogen atom of the viologen group respectively (Figure 21). Following this impregnation excess $Cr(acac)_3$ was adsorbed onto the

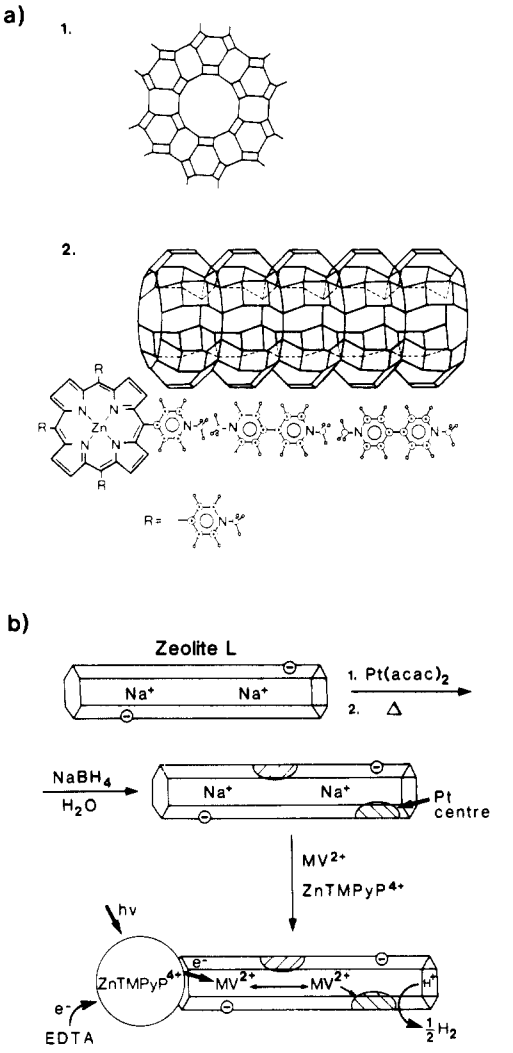

Figure 22. (a) Perspective view of (a) zeolite L showing the one-dimensional channel circumscribed by 12-membered rings and (b) the zeolite L main channel and $ZnTMPyP^{4+}$ and MV^{2+} ions. (b) Scheme outlining the photochemical production of hydrogen from water. Reprinted from ref 69; copyright 1987 American Chemical Society.

zeolite. This paramagnetic complex is substitution inert and too large to enter the pores of the zeolite and so can be expected to reside only on the outer surface. In Figure 21b it can be seen that a rapid relaxation of the upfield spins occurs while the downfield carbons are occluded by the zeolite and are not affected. Finally, the complex was exchanged into a zeolite already previously exchanged with Gd^{3+} which localizes on the inner surface. Attenuation of the peak due to the viologen group occurs while the other peak is unaffected (Figure 21c). The cation is only able to interact with this part of the complex. It can be concluded that half the molecule, the viologen end, resides in the zeolite while the larger $[Ru(bpy)_3]^{2+}$ resides outside the zeolite (Scheme 1).

Exchange of the cobalt and iron metallocene cations, $M(CpR)_2^+$ or $M(Cp)(CpR)^+$, into NaY zeolites yields concentrations of $(1–2) \times 10^{-5}$ mol/g of zeolite as determined by differences in the UV–vis spectra of the solutions before and after the exchange reaction.[67] Larger, substitution inert, $[Ru(bpy)_3]^{2+}$ or $[Os(bpy)_3]^{2+}$ can be similarly adsorbed onto the outer surfaces of these same zeolites. Concentrations of about (2–3) $\times$ 10^{-6} mol/g of zeolite are consistent with only surface

adsorption. Zeolites treated in this manner have been attached to SnO_2 electrodes using polystyrene films. Energy-dispersive X-ray emission spectra clearly show the presence of a cobalt metallocene species in the zeolite part of the film near the SnO_2 surface but not in the polystyrene overlayer. The rate of charge transfer between the entrapped metallocene and the electrode was found to increase by adsorbing the $[M(bpy)_3]^{2+}$ cations onto the outer surface of the zeolite. Oxidation and reduction of the metallocene are easy if the potentials of the surface and trapped species are similar. The mechanism likely involves rapid electron transfer between the surface-confined coordination complexes and the intrazeolite metallocenes; for example, the cathodic process can be represented as

$$\begin{array}{ccc} [Ru(bpy)_3]^{2+}(surf) + e^-(electrode) & \longrightarrow & [Ru(bpy)_3]^{+}(surf) \\ \uparrow & & + \\ [Ru(bpy)_3]^{2+}(surf) + [Co(CpCH_3)_2](bulk) & \longleftarrow & [Co(CpCH_3)_2]^{+}(bulk) \end{array}$$

Methylviologen cations can be exchanged into the bulk of zeolite Y while metalloporphyrin cations are exchanged onto the outer surface.[68] X-ray photoelectron and Auger electron spectroscopies were used to determine the location of the cations. Zeolite powders were exchanged with (1) 5×10^{-6} mol of cobalt tetrakis(*N*-methyl-4-pyridyl)porphyrin chloride ($CoTMPyP^{4+}$) and 1.9×10^{-4} mol of *N*-methyl-*N'*-propanesulfonato-4,4'-bipyridinium iodide ($MPVS^+$)/g of zeolite and (2) just 1.9×10^{-4} mol of $MPVS^+$/g of zeolite. For both samples a peak for sulfur was detected by XPS but not by AES. The difference may arise because the photoelectron escape depth is greater in the XPS experiment than in the AES experiment. These results indicate that with or without adsorbed metalloporphyrin cations the viologen cations lie near but not on the outer surface of the zeolite particles. The ^{13}C NMR spectrum of a D_2O suspension of a zeolite exchanged with methylviologen (MV^{2+}) and $ZnTMPyP^{4+}$ yields four resonances that can be assigned to bound MV^{2+}. The 500-Hz line width of these bands indicates that the MV^{2+} cations are not in solution but are inside the zeolite where they undergo hindered rotation. The concentration of surface-bound $ZnTMPyP^{4+}$ was below the detection limit of the NMR experiment. Electrodes coated with zeolites exchanged in this manner exhibit current rectification and charge-trapping reactions.

A similar array of molecules in and on zeolite L leads to an electron relay system capable of photochemically generating hydrogen from water.[69] The Na^+ cations within the one-dimensional channel of this zeolite are initially exchanged with $Pt(acac)_2$, which is reduced to platinum particles on the internal surface of the zeolite, as discussed earlier. Methylviologen (MV^{2+}) is then incorporated into the channels by ion exchange. Zinc tetrakis(*N*-methyl-4-pyridyl)porphyrin ($[ZnTMPyP]^{4+}$) is too large to enter the zeolite channels but it is strongly adsorbed on the outer surface.[68] Desorption of the porphyrin cations requires repeated back-exchange with saturated KCl or NaCl solutions. Loadings are consistent with 2–3 monolayer coverage of the zeolite surface. When this assembly is equilibrated with a 2.0×10^{-3} M EDTA solution at pH 4.0 and washed repeatedly, 2.5×10^{-6} mol of EDTA is adsorbed per gram of zeolite. The trimolecular system generated at the solution/zeolite interface under these conditions, EDTA–porphyrin–MV^{2+}, is an effective electron-transport chain that photochemically evolves hydrogen from water. The fluorescence decays are consistent with singlet-state electron-transfer quenching of $[ZnTMPyP]^{4+}$ by methylviologen.

F. Summary

Organometallic compounds and coordination complexes can be quantitatively located within the α-cages or channels of large-pore zeolites by either direct means or intrazeolite synthesis. Internal entrapment of the species is confirmed by using several methods: EPR changes induced by intrazeolite perturbations (Cp_2Cr), shifts of far-IR zeolite cation modes ($Co_2(CO)_8$), cation-induced mid-IR shifts of ligand modes ($CpIr(CO)_2$ and $Ni(CO)_4$), EPR spin-exchange relaxation effects by slurrying with a DPPH spin probe (paramagnetic bipyridine complexes), STEM, XPS surface-sensitive probes (phthalocyanines), size-dependent chemical reaction (phosphines with $Co_4(CO)_{12}$), intrazeolite catalytic poisoning reactions (phosphine effect on olefin hydrogenation by $ZORh(allyl)_2$, selective intrazeolite catalytic reactions (butadiene hydrogenation by $ZOMo(CO)_3$), and ^{13}C CPMAS NMR relaxation probes (linked $[Ru(bpy)_3]^{2+}$–$viologen^{2+}$, external $Cr(acac)_3$ and internal Gd^{3+}).

By judicious selection of the size, shape, and charge of organometallics and coordination complexes, these reagents can also be targeted to, and anchored on, the external regions of the zeolite (supramolecular organized assemblies of redox-active guests).

The homogeneity of a zeolite impregnation reaction is a question not as fully explored. The fast and homogeneous uptake of Brønsted acid functionalities by ferrocene in acid zeolites demonstrates this process. It can be assumed that similar types of molecules will also diffuse and locate uniformly. An even distribution of cationic guests can be assumed based on the requirement of charge balancing by the zeolite lattice. However, the distribution of sterically demanding guests still requires some scrutiny.

The field of intrazeolite organometallics is rapidly expanding. The applications of these systems have been only slightly touced upon in this article, namely, gas separation, electron-transport relays, and shape-selective catalysis. The ability to locate these compounds either inside or outside the zeolite lattice has been an important consideration in the intentional design and construction of these systems. The potential that many of these systems display in a wide range of applications clearly provides considerable incentive for further work.[60b,74]

Acknowledgments. We acknowledge the financial support of the Natural Sciences and Engineering Research Council of Canada's Operating and Strategic grants programs and the University Research Award Program of Imperial Oil, Canada. C.J.G. is grateful to the Ontario government for a graduate scholarship.

G. References

(1) Bailey, D. C.; Langer, S. H. *Chem. Rev.* **1981**, *81*, 109.
(2) Breck, D. W. *Zeolite Molecular Sieves*; Wiley: New York, 1974.

(3) *Zeolite Chemistry and Catalysis*; Rabo, J. A., Ed.; ACS Monograph 171; American Chemical Society: Washington, DC, 1976.
(4) (a) Jacobs, P. A. *Stud. Surf. Sci. Catal.* **1982**, *12*, 71. (b) Gallezot, P. *Catal. Rev.—Sci. Eng.* **1979**, *20*, 121.
(5) (a) Ballivet-Tkatchenko, D.; Tkatchenko, I.; Duc Chau, N. *Stud. Surf. Sci. Catal.* **1982**, *12*, 123. Reference 4.
(6) Ozin, G. A.; Godber, J. P.; Hugues, F.; Nazar, L. F. *J. Mol. Catal.* **1983**, *21*, 313.
(7) Zerger, R. P.; McMahon, K. C.; Seltzer, M. D.; Michael, R. D.; Suib, S. L. *J. Catal.* **1986**, *99*, 498.
(8) Che, M.; Richard, M.; Olivier, D. *J. Chem. Soc., Faraday Trans. 1* **1980**, *76*, 1526.
(9) Gallezot, P.; Primet, M.; Imelik, I. *Molecular Sieves II. ACS Symp. Ser.* **1977**, *No. 40*, 144.
(10) (a) Abdo, S.; Howe, R. F. *J. Phys. Chem.* **1983**, *87*, 1713. (b) *Ibid.* **1983**, *87*, 1722.
(11) Yong, Y. S.; Howe, R. F. *J. Chem. Soc., Faraday Trans. 1* **1986**, *82*, 2887.
(12) (a) Yong, Y. S.; Howe, R. F.; Hughes, A. E.; Jaeger, H.; Sexton, B. A. *J. Phys. Chem.* **1987**, *91*, 6331. (b) Anderson, S. L. T.; Howe, R. F. *J. Phys. Chem.* **1989**, *93*, 4913.
(13) Persaud, L.; Bard, A. J.; Campion, A.; Fox, M. A.; Mallouk, T. E.; Webber, S. E.; White, J. M. *Inorg. Chem.* **1987**, *26*, 3825.
(14) Okamoto, Y.; Maezawa, A.; Kane, H.; Imanaka, T. *J. Chem. Soc., Chem. Commun.* **1988**, 380.
(15) (a) Gelin, P.; Ben Taarit, Y.; Naccache, C. *J. Catal.* **1979**, *59*, 357. (b) Gelin, P.; Ben Taarit, Y.; Naccache, C. *J. Catal.* **1981**, *70*, 32. (c) Gelin, P.; Ben Taarit, Y.; Naccache, C.; Diab, Y. *Nouv. J. Chim.* **1984**, *8*, 675. (d) Lefebvre, F.; Ben Taarit, Y. *Nouv. J. Chim.* **1984**, *8*, 387. (e) Burkhardt, I.; Gutschick, D.; Lohse, U.; Miessner, H. *J. Chem. Soc., Chem. Commun.* **1987**, 291. (f) Takahashi, N.; Mijin, A.; Ishikawa, T.; Nebuka, K.; Suematsu, H. *J. Chem. Soc., Faraday Trans. 1* **1987**, *83*, 2605.
(16) Gelin, P.; Lefebvre, F.; Elleuch, B.; Ben Taarit, Y.; Naccache, C. *Intrazeolite Chemistry*; Stucky, G. D., Dwyer, F. G., Eds.; ACS Symp. Ser. 218; American Chemical Society: Washington, DC, 1983.
(17) Gelin, P.; Ben Taarit, Y.; Naccache, C. *Stud. Surf. Sci. Catal.* **1981**, *7*, 898.
(18) Hanson, B. E.; Davis, M. E.; Taylor, D.; Rode, E. *Inorg. Chem.* **1984**, *23*, 52.
(19) Basset, J. M.; Theolier, A.; Commereuc, D.; Chauvin, Y. *J. Organomet. Chem.* **1985**, *279*, 147.
(20) Ballivet-Tkatchenko, D.; Coudurier, G. *Inorg. Chem.* **1979**, *18*, 558.
(21) (a) Ballivet-Tkatchenko, D.; Coudurier, G.; Mozzanegg, H. *Stud. Surf. Sci. Catal.* **1980**, *5*, 309. (b) Ballivet-Tkatchenko, D.; Tkatchenko, I. *J. Mol. Catal.* **1981**, *13*, 1.
(22) Bein, T.; Jacobs, P. A. *J. Chem. Soc., Faraday Trans. 1* **1983**, *79*, 1819.
(23) Bein, T.; Jacobs, P. A. *J. Chem. Soc., Faraday Trans. 1* **1984**, *80*, 1391.
(24) Bein, T.; Schmidt, F.; Gunsser, W.; Schmiester, G. *Surf. Sci.* **1985**, *156*, 57.
(25) Schneider, R. L.; Howe, R. F.; Watters, K. L. *Inorg. Chem.* **1984**, *23*, 4600.
(26) Connaway, M. C.; Hanson, B. E. *Inorg. Chem.* **1986**, *25*, 1445.
(27) Ozin, G. A.; Godber, J. P. In Intrazeolite Organometallics: Spectroscopic Probes of Internal Versus External Confinement of Metal Guests. *Excited States and Reactive Intermediates: Photochemistry, Photophysics, and Electrochemistry*; Lever, A. P. B.;, Ed.; ACS Symposium Series 307; American Chemical Society: Washington, DC, 1986.
(28) Newcomb, T. P.; Gopal, P. G.; Watters, K. L. *Inorg. Chem.* **1987**, *26*, 809.
(29) Olivier, D.; Richard, M.; Che, M. *Chem. Phys. Lett.* **1978**, *60*, 77.
(30) Derouane, E. G.; Nagy, J. B.; Vedrine, J. C. *J. Catal.* **1977**, *46*, 434.
(31) Bein, T.; McLain, S. J.; Corbin, D. R.; Farlee, R. D.; Moller, K.; Stucky, G. D.; Woolery, G.; Sayers, D. *J. Am. Chem. Soc.* **1988**, *110*, 1801.
(32) Brown, T. L. *J. Mol. Catal.* **1981**, *12*, 41.
(33) (a) Edgell, W. F.; Lyford, J. *J. Am. Chem. Soc.* **1971**, *93*, 6407. (b) Panel, K. H.; Jackson, D. *J. Am. Chem. Soc.* **1976**, *98*, 4443. (c) Darensbourg, M. Y.; Barros, H. C. *Inorg. Chem.* **1979**, *18*, 3286. (d) Edgell, W. F.; Chanjamsri, S. *J. Am. Chem. Soc.* **1980**, *102*, 147.
(34) Borvornwattananont, A.; Moller, K.; Bein, T. *J. Phys. Chem.* **1989**, *93*, 4205.
(35) Herron, N.; Stucky, G. D.; Tolman, C. A. *Inorg. Chim. Acta* **1985**, *100*, 135.
(36) Ozin, G. A.; Haddleton, D. M.; Gil, C. J. *J. Phys. Chem.* **1989**, *93*, 6710.
(37) Lechert, H.; Wittern, K. P.; Schweitzer, W. *Acta Phys. Chem.* **1978**, *24*, 201.
(38) Ozin, G. A.; Gil, C. J., unpublished results; Gil, C. J. M.Sc. Thesis, University of Toronto, 1988.
(39) Schuster-Woldan, H. G.; Basolo, F. *J. Am. Chem. Soc.* **1966**, *88*, 1657.
(40) Cramer, R. *J. Am. Chem. Soc.* **1964**, *86*, 217.
(41) Borvornwattananont, A.; Moller, K.; Bein, T. *J. Phys. Chem.* **1989**, *93*, 4562.
(42) Pichat, P. *J. Phys. Chem.* **1975**, *79*, 2127.
(43) Huang, Y. *J. Catal.* **1980**, *61*, 461.
(44) Michalik, J.; Narayana, M.; Kevan, L. *J. Phys. Chem.* **1984**, *88*, 5237.
(45) Cruz, W. V.; Leung, P. C. W.; Seff, K. *J. Am. Chem. Soc.* **1978**, *100*, 6997.
(46) Lunsford, J. H. *Catal. Rev.—Sci. Engl.* **1975**, *12*, 137.
(47) Mochida, I.; Kato, A.; Seiyama, T. *Bull. Chem. Soc. Jpn.* **1972**, *45*, 2230.
(48) Peigneur, P.; Lunsford, J. H.; DeWilde, W.; Schoonheydt, R. A. *J. Phys. Chem.* **1977**, *81*, 1179.
(49) Ganzerla, R.; Pinna, F.; Lenarda, M.; Graziani, M. *J. Organomet. Chem.* **1983**, *222*, 183.
(50) Howe, R. F.; Lunsford, J. H. *J. Phys. Chem.* **1975**, *79*, 1836.
(51) Dai, P. S. E.; Lunsford, J. H. *Inorg. Chem.* **1980**, *19*, 262.
(52) DeWilde, W.; Lunsford, J. H. *Inorg. Chim. Acta* **1979**, *34*, L229.
(53) Quayle, W. H.; Peeters, G.; DeRoy, G. L.; Vansant, E. F.; Lunsford, J. H. *Inorg. Chem.* **1982**, *21*, 2226.
(54) Mizuno, K.; Lunsford, J. H. *Inorg. Chem.* **1983**, *22*, 3484.
(55) Koichi, M.; Imamura, S.; Lunsford, J. H. *Inorg. Chem.* **1984**, *23*, 3510.
(56) Imamura, S.; Lunsford, J. *Langmuir* **1985**, *1*, 326.
(57) Herron, N. *Inorg. Chem.* **1986**, *25*, 4714.
(58) Drago, R. S.; Bresinska, I.; George, J. E.; Ballus, K., Jr.; Taylor, R. J. *J. Am. Chem. Soc.* **1988**, *110*, 304.
(59) Meyer, G.; Wohrle, D.; Mohl, M.; Schulz-Ekloff, G. *Zeolites* **1984**, *4*, 30.
(60) (a) Herron, N.; Stucky, G. D.; Tolman, C. A. *J. Chem. Soc., Chem. Commun.* **1986**, 1521. (b) Herron, N. *CHEMTECH* **1989**, 542.
(61) Woltermann, G. H.; Durante, V. A. *Inorg. Chem.* **1983**, *22*, 1954.
(62) Huang, T.; Schwartz, J. *J. Am. Chem. Soc.* **1982**, *104*, 5244.
(63) Corbin, D. R.; Seidel, W. C.; Abrams, L.; Herron, N.; Stucky, G. D.; Tolman, C. A. *Inorg. Chem.* **1985**, *24*, 1800.
(64) Ozin, G. A.; Godber, J. *J. Phys. Chem.* **1989**, *93*, 878.
(65) Dutta, P. K.; Zaykoski, R. E.; Thomson, M. A. *Zeolites* **1986**, *6*, 423.
(66) Richardson, B. R.; Haw, J. F.; Mallouk, T. E., to be submitted for publication.
(67) Li, Z.; Mallouk, T. E. *J. Phys. Chem.* **1987**, *91*, 643.
(68) Li, Z.; Wang, C. M.; Persaud, L.; Mallouk, T. E. *J. Phys. Chem.* **1988**, *92*, 2592.
(69) Persaud, L.; Bard, A. J.; Campion, A.; Fox, M. A.; Mallouk, T. E.; Webber, S. E.; White, J. M. *J. Am. Chem. Soc.* **1987**, *109*, 7309.
(70) Ozin, G. A.; Godber, J.; Baker, M. D. *J. Phys. Chem.* **1989**, *93*, 2899.
(71) Suib, S. L.; Bordelanu, O. G.; McMahon, K.; Psaras, D. ACS Symp. Ser. 177; American Chemical Society: Washington, DC, 1982; pp 225–238.
(72) (a) Susic, M. V. *Electrochim. Acta* **1979**, *24*, 535. (b) Pereira-Rames, J. P.; Messina, R.; Perichon, J. *Electroanal. Chem.* **1983**, *146*, 157.
(73) Gallezot, P. In *Metal Clusters*; Moskovits, M., Ed.; Wiley: New York, 1986; p 219 and references cited therein.
(74) Ozin, G.; Stein, A.; Kuperman, A. *Advanced Materials. Angew. Chem., Int. Ed. Engl.* **1989**, *101*, 373 and references cited therein.